Mechanisms involved in AMPK-mediated deposition of tight junction components to the plasma membrane

Jingshing Wu[1], Pascal Rowart[2], Francois Jouret[2], Brandon M. Gassaway[1,3], Vanathy Rajendran[1], Jesse Rinehart[1,3], Michael J. Caplan[1*]

From the [1]Department of Cellular and Molecular Physiology, Yale School of Medicine, New Haven, CT; [2]Groupe Interdisciplinaire de Génoprotéomique Appliquée (GIGA), Cardiovascular Sciences, University of Liège (ULiège), Avenue de L'Hôpital 11, 4000 Liège, Belgium; [3]Systems Biology Institute, Yale University, West Haven, CT

Running title: *AMPK-mediated deposition of tight junction components*

*To whom correspondence should be addressed: Michael J. Caplan: Department of Cellular and Molecular Physiology, Yale School of Medicine, P.O. Box 208026, New Haven, CT-06520-8026; michael.caplan@yale.edu; Tel.: (203) 785-7316; Fax. (203) 785-4951.

Key words: Tight junction, adherens junction, afadin, zonula occludens (ZO)-1, AMP activated protein kinase (AMPK), atypical protein kinase C (aPKC), Cdc42, Par3

ABSTRACT

AMP activated protein kinase (AMPK) activation promotes early stages of epithelial junction assembly. AMPK activation in MDCK renal epithelial cells facilitates localization of the junction-associated proteins aPKC and Par3 to the plasma membrane and promotes conversion of Cdc42, a key regulator of epithelial polarization and junction assembly, to its active GTP bound state. Furthermore, Par3 is an important regulator of AMPK-mediated aPKC localization. Both aPKC and Par3 serve as intermediates in AMPK-mediated junction assembly, with inhibition of aPKC activity or Par3 knockdown disrupting AMPK's ability to facilitate zonula occludens (ZO-1) localization. AMPK phosphorylates the adherens junction protein afadin and regulates its interaction with the tight junction protein zonula occludens (ZO)-1. Afadin is phosphorylated at two critical sites, S182 (residing within an aPKC consensus site) and S1049 (residing within an AMPK consensus site), that are differentially regulated during junction assembly and that exert different effects on the process. Expression of phospho-defective mutants (S182A and S1082A) perturbed ZO-1 localization to the plasma membrane during AMPK-induced junction assembly. Expression of S182A increased the ZO-1/afadin interaction, while S1049A reduced this interaction during extracellular calcium-induced junction assembly. Inhibition of aPKC activity also increased the ZO-1/afadin interaction. Taken together, these data suggest that aPKC phosphorylation of afadin terminates the ZO-1/afadin interaction, and thus permits the later stages of junction assembly.

Epithelial cells serve as barriers that separate different tissues and body compartments from one another. These barriers both protect an organism from its external environment and mediate the import and export of substances, often against steep concentration gradients. Epithelial cells are attached to one another through highly specialized protein complexes that constitute a variety of intercellular junctions, including tight junctions (TJs) and adherens junctions (AJs) (1). These junctions work together to not only facilitate adhesion between the lateral domains of adjacent cells but also to help to establish cell polarity (2).

The assembly of junction complexes is an early and critical step in the organization of individual epithelial cells into an intact, polarized and functionally competent monolayer epithelium. Hundreds of transmembrane and cytoplasmic proteins have been identified that dynamically interact with each other to promote adherens and tight junction assembly and maturation (3). One obligate scaffolding protein includes zonula occludens-1 (ZO-1), which itself has been shown to potentially interact with more than 400 proteins (4). During the early stages of

junction assembly, ZO-1 localizes to the nascent adherens junction, where it associates with the AJ scaffolding protein afadin—an interaction critical for the assembly and maturation of AJs and TJs (5). In association with junction maturation, ZO-1 dissociates from afadin and translocates to the tight junction, where it tethers transmembrane tight junction proteins to the actin cytoskeleton (5,6).

Much remains unknown about the molecular mechanisms that promote the formation of AJs and TJs, including the nature of the cellular machinery that regulates the ZO-1-afadin association. Previous observations from our group and others demonstrate that in the Madin-Darby canine kidney (MDCK) epithelial cell model, AMP-activated kinase (AMPK) plays an active role in initiating transient junction formation by specifically phosphorylating afadin *in vitro* and increasing the level of afadin bound to ZO-1 (7-10). AMPK plays important roles in the cellular response to energy deprivation and has been implicated in processes that contribute to epithelial polarization (10,11).

Additional regulators of AJ and TJ formation include the atypical protein complex C (aPKC)-Par3-Par6 complex proteins. aPKC phosphorylates several AJ and TJ proteins to promote their stable localization at the plasma membrane (12-14). aPKC interacts with the Par polarity proteins Par3 and Par6, which serve as scaffolding proteins to coordinate the proper localization of aPKC during junction assembly (15). Regulation of aPKC activation may occur via at least two different mechanisms: relief of Par6 suppression of aPKC activity through GTP-bound Cdc42 as well as through phosphorylation of a PKC by upstream kinases (16,17). GTP-bound Cdc42 is important for junction assembly and inactivation of aPKC kinase activity during epithelial polarization (18,19). The knockdown of aPKC, Par3, or Par6 have each been individually shown to prevent ZO-1 and afadin localization to sites of cell-cell contact (20).

Here, we sought to further elucidate the mechanisms through which AMPK regulates junction assembly and to explore the relationship between AMPK and aPKC-mediated events. We report for the first time that AMPK promotes both Par3 and aPKC localization to the plasma membrane during junction assembly and that aPKC inhibition prevents AMPK-mediated junction assembly by affecting the ZO-1/afadin interaction. We also analyzed afadin phosphorylation and identified residues that are important for the ZO-1/afadin interaction. Thus, our results demonstrate that AMPK-mediated junction assembly is dynamic and involves the participation of many junction proteins, with aPKC performing as a central player in this process.

Results

AMPK regulates aPKC localization during junction assembly

In the MDCK epithelial cell model system, the presence of extracellular Ca^{2+} is critical for the formation and maintenance of intercellular junctions. Exposure to low concentrations of extracellular Ca^{2+} disrupts intercellular junctions while the restoration of Ca^{2+} to normal concentration levels leads to the deposition of junction proteins at sites of cell-cell attachment (2,21). This manipulation has come to be known as the "Ca^{2+} switch." Consistent with our previous findings, we were able to demonstrate that the Ca^{2+} switch promotes AMPK phosphorylation (Supplemental Figure 1A) (8,9,22). We employed this paradigm in experiments designed to assess whether AMPK regulates aPKC during junction formation. AMPK is a heterotrimer, requiring the proper assembly of all three subunits together to be functionally active. The knockdown of one subunit is thus sufficient to ablate AMPK activity. Expression of AMPK subunit isoforms differs among tissues and we targeted the α1 subunit of AMPK, which is the predominant α subunit isoform expressed in MDCK cells, to achieve effective knockdown of AMPK function (AMPK α1 KD) in our studies (23). A short hairpin (sh) RNA construct targeting AMPK's α1 subunit was stably transfected into MDCK cells. The efficacy of this approach has been previously demonstrated (22). Control cells were created by transfecting MDCK cells with an empty vector (referred to as AMPK WT cells). Previous studies from our lab have demonstrated that AMPK knockdown in cultured cells affects the rate of ZO-1 localization to the plasma membrane during

tight junction formation and decreases the magnitude of the transepithelial resistance (9).

We first examined whether AMPK activation could regulate aPKC localization by performing immunofluorescence studies to monitor aPKC deposition at the plasma membrane. We cultured AMPK α1 KD and AMPK WT cells to confluency in normal Ca^{2+} media (1.8 mM Ca^{2+}, NCM) before incubating them in low Ca^{2+} media (5 μM Ca^{2+}, LCM) for 16h. Following the reintroduction of NCM for 2 hours (the "Ca^{2+} switch or CS), cells were fixed for immunofluorescence studies. We found that, following incubation in LCM for 16h, aPKC was diffusely localized throughout the cytoplasm in both AMPK WT and KD cells (Fig. 1A). We observed that following the Ca^{2+} switch, the quantity of aPKC that was distributed at the plasma membrane in control cells was significantly higher than that observed in AMPK KD cells (Fig. 1A, B). The increase in aPKC localization to the plasma membrane in AMPK WT cells in response to the calcium switch was consistent with what we observed in WT MDCK cells subjected to the calcium switch for one hour (Fig. 1C, D). We found that there was no difference in the quantity of aPKC protein expression in AMPK WT versus KD cells under steady state, LCM, or calcium switch conditions (Supplemental Fig. 2A, B). Examination of confocal z-stack images also demonstrated that aPKC and ZO-1 co-localized with one another during the calcium switch, confirming previously published reports (24) (Supplemental Figure 3). These results indicate that AMPK expression plays an important role in regulating aPKC localization during Ca^{2+} switch-mediated junction assembly. To determine whether AMPK activity is involved in regulating aPKC localization, we monitored whether pharmacological activation of AMPK by 2mM 5-aminoimidizole-4 carboxamide riboside (AICAR), an AMPK activator, for 2h would also promote aPKC localization to the plasma membrane. We cultured MDCK cells to confluency in NCM before subjected them to LCM for 16 hours. AICAR (2 mM) was then introduced in LCM for 1h (LCM+AICAR). Following AICAR treatment, we observed a significant increase in the number and length of strands of aPKC labeling located at the plasma membrane without any changes in aPKC expression (Fig. 1C, D and Supplemental Fig. 2C). AMPK activation was verified by assessing the level of AMPK phosphorylation following AICAR treatment (Supplemental Figure 1A, B). Taken together, the AMPK KD and AICAR results indicate that AMPK activity is involved in regulating aPKC localization during junction assembly.

To probe how AMPK regulates aPKC localization and function, we monitored whether AMPK similarly controls the distributions and activities of two critical regulators of aPKC activity and localization, Cdc42 and Par3. When in its GTP-bound form, Cdc42 upregulates aPKC activity and promotes aPKC apical membrane localization (25-27). Consequently, we measured whether AMPK affects the level of Cdc42-GTP. We performed the Ca^{2+} switch manipulation on AMPK α1 KD and AMPK WT for 2 hours before lysing the cells and measuring Cdc42-GTP levels by using pull-down assays that employ the GST-Pak1 effector domain as an affinity reagent that interacts specifically with GTP bound but not GDP bound Cdc42 (28,29). We found that, despite similar levels of total Cdc42 expression at steady state and during the calcium switch, control cells exhibited a robust increase in Cdc42-GTP levels in response to the Ca^{2+} switch at 2h, whereas AMPK KD cells failed to display a similar increase (Fig. 2A, B and Supplemental Fig. 2A, B). In fact, Cdc42-GTP levels were similar between LCM and Ca^{2+} switch conditions in AMPK KD cells, suggesting that AMPK is a significant regulator of the formation of Cdc42-GTP during Ca^{2+}-induced junction assembly (Fig. 2A, B). The increase in Cdc42-GTP levels in AMPK WT cells subjected to the calcium switch was consistent to what we found in WT MDCK cells (Fig. 2C, D). To further evaluate the role of AMPK in this process, we next analyzed whether AMPK activation in an LCM environment alone is sufficient to promote Cdc42 nucleotide exchange leading to increases in the levels of GTP-bound Cdc42. WT MDCK cells grown to confluence in NCM were incubated in LCM for 16h before being exposed to 2mM AICAR for 2h (LCM+AICAR). We found that AMPK activation resulted in a 2-fold increase in Cdc42-GTP levels without affecting total level of Cdc42 expression (Fig. 2C, D and Supplemental

Fig. 2C). The magnitude of the increase observed was comparable to that achieved during the Ca^{2+} switch (Fig. 2C, D). To ensure that the effects of AICAR were mediated by AMPK, we analyzed the effect of AICAR on Cdc42-GTP levels in AMPK KD cells and found that these cells failed to exhibit an increase Cdc42-GTP in response to AICAR treatment (Fig. 2A, B). Taken together, these studies support the conclusion that AMPK expression and activity play important roles in promoting the formation of Cdc42-GTP during junction assembly.

Par3 is an important scaffolding protein that localizes to the nascent adherens junction during the early stages of junction assembly, subsequently transitioning to a predominantly tight junction distribution when junctions have matured (30,31). Following Cdc42-GTP-mediated aPKC activation, aPKC interacts with Par3 and the protein complex is subsequently recruited to primordial junctions (12,32). Our confocal imaging experiments reveal that Par3 and ZO-1 co-localized with one another during the calcium switch (Supplemental Figure 3). We subsequently evaluated Par3's role during junction assembly by monitoring the effects of shRNA-mediated Par3 knockdown (Par3 KD) on calcium-switch mediated junction assembly (Supplemental Figure 2D). Both Par3 KD cells and their WT counterparts were subjected to the calcium switch and ZO-1 localization was monitored by immunofluorescence. We observed that the length of ZO-1 localization at the plasma membrane was significantly decreased in Par3 KD cells compared to control cells, demonstrating that Par3 contributes to ZO-1 localization during junction assembly (Fig. 3A, B).

To determine whether AMPK could regulate Par3 localization, we performed the Ca^{2+} switch manipulation on AMPK α1 KD and AMPK WT cells for 2h before monitoring Par3 deposition through immunofluorescence analysis. We found that, following incubation in LCM for 16h, Par3 was diffusely localized throughout the cytoplasm while the level of total Par3 protein expression remained unchanged during both steady state and calcium switch conditions (Supplemental Figs. 2A, 2B, and 3). We also observed that, following the Ca^{2+} switch, Par3 was localized at the plasma membrane to a significantly lesser extent in AMPK α1 KD cells as compared to control cells. These results indicate that AMPK expression is involved in regulating Par3 localization during Ca^{2+} switch-mediated junction assembly (Supplemental Fig. 4). The increase in Par3 localization at the plasma membrane in AMPK WT cells during the calcium switch is consistent with what we found in WT MDCK cells (Fig. 4A, B). To determine if AMPK activity plays a role regulating Par3 localization, we monitored whether activation of AMPK by 2mM AICAR for 2h could also promote Par3 localization to the plasma membrane in cells that were maintained in LCM (Fig. 4A, B). MDCK cells were cultured to confluency in NCM before being subjected to LCM for 16 hours. 2 mM AICAR was introduced for 2h (LCM+AICAR) prior to immunofluorescence analysis. We found that, following AICAR treatment, there was a significant increase in the number and length of strands labeling for Par3 located at the plasma membrane without any changes in the level of Par3 protein expression (Fig. 4A, B and Supplemental Fig. 2C). These results confirm that AMPK activity plays an important role in regulating Par3 localization during junction assembly.

To assess whether Par3 acts as an intermediate in AMPK-mediated junction assembly, we first monitored the effects of Par3 KD on ZO-1 localization. We again promoted AMPK-mediated junction assembly by treating Par3 KD or control cells incubated in LCM for 16 hours with 2 mM AICAR for 2 hours. Compared to activity in control cells, we found that ZO-1 localization at the plasma membrane was significantly decreased in Par3 KD cells exposed to LCM+AICAR conditions (Figure 3C, D). These results indicate that Par3 is an important intermediate in AMPK-mediated junction assembly.

aPKC inhibition prevents AMPK-mediated junction assembly and increases the association between ZO-1 and afadin

Since our studies show that AMPK regulates aPKC localization to the plasma membrane and may control aPKC activity through promotion of the formation of Cdc42-GTP, we next sought to ascertain whether aPKC plays a role in AMPK-mediated junction assembly by determining the

effects of aPKC inhibition on this process. We used a cell-permeable myristoylated pseudosubstrate inhibitor of aPKC activity to pharmacologically inhibit aPKC (33-35). We first monitored the effects of aPKC inhibition during the Ca^{2+} switch to test the efficacy of the inhibitor. MDCK cells grown to confluence were incubated in LCM for 16h prior to being pre-treated for 2h with or without 10μM or 25μM aPKC inhibitor in LCM. NCM was introduced for another 2h in the continued presence of the inhibitor. In concert with what has been previously reported, we found that aPKC inhibition at 10μM was sufficient to partially prevent Ca^{2+} switch-mediated junction assembly and that this effect occurred in a dose-dependent manner (Fig. 5A, B) (13,36). We and others have previously found that the Ca^{2+} switch maneuver induces AMPK activation, as evidenced by its phosphorylation at Thr 172 on its α subunit (8,10). Inhibition of aPKC activity did not affect this Ca^{2+} switch induced AMPK phosphorylation (Fig. 5D). To monitor the role of aPKC in AMPK-mediated junction assembly, MDCK cells grown to confluency were again incubated in LCM for 16h, then pre-treated for 2h with or without 10μM aPKC inhibitor in LCM before being subject to AMPK activation by 2mM AICAR in the continued presence or absence of the aPKC inhibitor. We observed that, compared to cells treated with AICAR alone, those incubated in the presence of aPKC inhibitor with AICAR had a significantly lower level of ZO-1 distributed at the plasma membrane (Fig. 5A, C). This result suggests that AMPK-mediated junction assembly requires aPKC activity.

We have previously reported that AMPK activation promotes the formation of an interaction between ZO-1 and afadin (8). Since the data presented here indicate that aPKC acts downstream of AMPK to regulate junction assembly, we further probed whether these functional activities converge within one pathway. We specifically monitored whether aPKC is a regulator of the AMPK-mediated ZO-1/afadin interaction by assessing whether inhibition of aPKC activity alters the extent of this interaction. MDCK cells were grown to confluence before being incubated in LCM for 16h. Cells were pre-treated with or without 10μM aPKC inhibitor for 2h before 2mM AICAR was introduced for another 2h in the continued presence or absence of the inhibitor. To measure the level of ZO-1/afadin interaction, we performed co-immunoprecipitation studies in which endogenous afadin was immunoprecipitated using an antibody directed against afadin and the quantity of co-precipitating ZO-1 was subsequently assessed by western blotting using an antibody directed against the endogenous ZO-1 protein. In these studies, AMPK activation by AICAR led to an increase in the ZO-1/afadin interaction (Fig. 5E, F). Inhibition of aPKC further increased the level of the ZO-1/afadin interaction during both the LCM incubation and following AMPK activation by AICAR as compared to that observed under similar conditions when aPKC activity was not inhibited (Fig. 5E,F). These results indicate that aPKC inhibition increases the extent of the interaction between ZO-1 and afadin specifically when adherens and tight junctions are not present (LCM conditions) and during AMPK-mediated junction assembly (LCM + AICAR conditions). Inhibition of aPKC did not significantly affect the extent of the ZO-1/afadin interaction during the Ca^{2+} switch, suggesting that the interaction may reach its maximal level during the Ca^{2+} switch or there may be additional mechanisms that also regulate the interaction and that are unaffected by aPKC inhibition (Fig. 5G, H).

Afadin phosphorylation at S228 and S1102 are regulators of junction assembly

Since protein phosphorylation is a common regulator of protein activity, we investigated how the ZO-1/afadin interaction is controlled by afadin phosphorylation. We first probed for whether afadin phosphorylation is changed during the Ca^{2+} switch relative to LCM conditions by using Phos-tag acrylamide containing gels in concert with western blotting. The Phos-tag reagent binds to phosphate groups, and its addition to acrylamide gels permits separation of proteins based on molecular weight as well as upon phosphorylation status (37). Proteins that are more heavily phosphorylated migrate at a slower rate in acrylamide gels containing the Phos-tag than their non-phosphorylated counterparts. We found that afadin phosphorylation robustly increased in response to the Ca^{2+} switch (Fig. 6A).

To identify the specific afadin residues phosphorylated during the Ca^{2+} switch and to assess whether phosphorylation at these residues is differentially regulated by this manipulation, we used a stable isotope dimethyl labeling quantitative proteomics strategy (38). Afadin was immunoprecipitated from cells maintained in LCM only or from LCM-incubated cells that were subjected to the Ca^{2+} switch, and the resulting immunoprecipitates were separated by SDS-PAGE. In-gel trypsin digestion followed by dimethyl labeling was performed, with samples subjected to the Ca^{2+} switch labeled with CD_2O and LCM samples labeled with CH_2O prior to being mixed in a 1:1 ratio (39). Phosphorylated peptides were enriched by TiO_2 binding prior to analysis by mass spectrometry (40). Relative phosphopeptide abundance was normalized according to the median value of the relative abundance of all non-phosphorylated afadin peptides within the same sample. While there were many sites on afadin that were found to be phosphorylated, two residues were of significant interest: S228 and S1102 (Supplemental Figure 5). The peptide that includes the S1102 residue contains the consensus sequence for AMPK recognition (41). While phosphorylation at this site was previously determined to be promoted by AMPK activation, in the present study we did not detect any changes in the phosphorylation level of S1102 in response to the Ca^{2+} switch manipulation (Table 1) (8). In contrast, S228 displayed an upregulation in its phosphorylation level in response to the Ca^{2+} switch by 1.703-fold (CI: 1.399-2.007). The peptide that contains the S228 residue also bears the consensus sequence for aPKC recognition (41).

Since phosphorylation at S228 and S1102 may be important for aspects of junction assembly, we sought to determine whether phosphorylation at either of these sites is important for regulating ZO-1 localization or for the interaction between afadin and ZO-1. We investigated the role of S228 and S1102 phosphorylation by generating phospho-defective mutant forms of afadin, in which these residues were individually replaced with alanine residues. These mutations were introduced into constructs containing the *mus musculus* cDNA sequence for HA-tagged afadin at either the S216 or S1083 sites (which correspond with the S228 and S1102 sites in *canis familiaris* afadin) and the constructs were stably transfected into wild-type MDCK cells. As a control, a construct encoding the HA-tagged wild-type *mus musculus* cDNA sequence afadin was also stably transfected into wild-type MDCK cells. Under steady state conditions, HA-tagged wild-type, S216A, and S1083A afadin localized to the plasma membrane (Supplemental Fig. 6A). The total level of afadin expression was increased by approximately 50% in cells expressing wild-type afadin and to a similar extent in cells expressing S216A mutant afadin compared to cells transfected with empty vector (Supplemental Fig. 6B, C). Total afadin expression was increased by ~200% in cells expressing the HA-tagged S1083A afadin mutant as compared to cells transfected with an empty vector (Supplemental Fig. 6B, C).

To assess whether and how the absence of phosphorylation at afadin residues S216 and S1083 might impact junction assembly, we monitored whether expression of these mutant afadin proteins affected the localization of ZO-1 during the Ca^{2+} switch and AMPK-mediated junction assembly. Confluent MDCK cells stably transfected with constructs containing HA-tagged wild-type afadin or afadin carrying the S216A or S1083A mutations were subject to the Ca^{2+} switch or 2mM AICAR treatment for 2h, and ZO-1 localization was monitored by immunofluorescence. We found that the introduction of the S216A mutation leads to a decrease in ZO-1 translocation to the plasma membrane following AICAR treatment but did not perturb ZO-1 localization in response to the Ca^{2+} switch (Fig. 6B, C, and D). The distribution of ZO-1 to the plasma membrane was found to be significantly lower in cells expressing S1083A HA-tagged afadin during both the Ca^{2+} switch as well as in response to AMPK activation by AICAR compared to those detected in cells expressing HA-tagged wild-type afadin (Fig. 6E, F, and G). Since the endogenous afadin is still expressed in these cells, it appears that the expression of the S216A or S1083A mutant afadin may exert a dominant-negative effect during junction assembly. However, additional mechanisms initiated by the Ca^{2+} switch may also be able to compensate for the dominant-negative properties of the S216A mutant protein. Together, these results suggest that

phosphorylation at S216 or S1083A of *mus musculus* afadin play modulatory roles during junction assembly.

Since afadin's interaction with ZO-1 is important for junction assembly, we also assessed whether S228 or S1102 phosphorylation affects afadin's ability to interact with ZO-1. Using the same MDCK cells stably transfected with HA-tagged wild-type afadin or afadin containing the S216A or S1083A mutation, we measured the extent of the ZO-1/HA-afadin interaction in response to the Ca^{2+} switch by performing co-immunoprecipitation experiments. In the following studies, HA-tagged afadin was immunoprecipitated using an antibody directed against the HA epitope tag and the level of endogenous ZO-1 that interacts with the HA-tagged afadin was monitored by western blotting. The calcium switch was performed for 2 hours in MDCK cells transfected with one of the HA-tagged constructs. In cells expressing the wild type HA-tagged afadin construct, we observed an increase in the ZO-1/HA-tagged afadin interaction in response to the Ca^{2+} switch relative to LCM levels, consistent with the behavior of endogenous afadin (Fig. 7A, B). Using the same experimental setup, we found that in MDCK cells expressing HA-tagged afadin that contains the S216A mutation, the extent of the ZO-1/HA-tagged afadin interaction was substantially larger during the LCM incubation relative to cells transfected with wild-type afadin (Fig. 7A, B). The extent of this interaction was not further increased by the Ca^{2+} switch (Fig. 7A, B). In contrast, in cells expressing S1083A afadin, we observed a low level of interaction between ZO-1 and afadin under LCM incubation conditions that remained low despite Ca^{2+} switch (Fig. 7C, D). These results indicate that during the Ca^{2+} switch, the absence of phosphorylation at the 216 residue in *mus musculus* afadin may promote the interaction between ZO-1 and afadin. Phosphorylation at S216 and S1083 appear to exert opposite effects on the interaction between afadin and ZO-1. While the ability to become phosphorylated at S1083 appears to be important in initiating a Ca^{2+} switch induced association between ZO-1 and afadin, phosphorylation at S216 appears to be required for the termination of this association that accompanies the later stages of junction formation and maturation. Loss of the capacity to become phosphorylated at S216 results in the formation of a stable interaction between ZO-1 and afadin that persists independent of the presence of extracellular calcium and of the stimuli that induce junction assembly.

Discussion

Epithelial adherens and tight junction assembly is a complex and incompletely understood process that involves cooperation between numerous proteins and the coordination of many different signaling pathways. Since perturbations in junction structure and functions are important features of a number of pathophysiological conditions, including inflammatory bowel disease, ischemic acute kidney injury, and cancer metastasis (42-44), it is important to understand the processes that promote junction integrity. Although AMPK is a well-known regulator of cell polarity, the relevant signaling pathways that participate up-or downstream of AMPK in epithelial polarization are currently still unclear. The work presented here was designed to expand our understanding of the proteins that participate downstream of AMPK to regulate AMPK-mediated adherens and tight junction assembly.

Since the aPKC/Par3/Cdc42 polarity complex proteins are central regulators of junction assembly and cell polarity, we explored whether and how AMPK influences and is influenced by these proteins in exerting its effects on junction formation (45). We found that AMPK serves as an upstream regulator of the aPKC/Par3/Cdc42 localizations and activities of components of this critical polarity complex. Furthermore, we find that AMPK and aPKC may phosphorylate afadin at S1102 and S228, respectively, to coordinate their antagonistic roles regulating the ZO-1/afadin interaction and to ultimately promote junction assembly. Taken together, these results not only reaffirm that AMPK plays a significant role regulating the development of the adherens and tight junction, but that the signaling mechanism downstream of AMPK is complex and dynamically regulated.

Our data indicate that AMPK is responsible for promoting the localization of both aPKC and Par3 to the plasma membrane and for regulating

the level of GTP-bound Cdc42. These results indicate that AMPK is an upstream regulator for both aPKC and Par3 localization to the plasma membrane during calcium switch-induced junction assembly. It remains to be determined whether additional intermediate proteins are involved in these functional interactions. Since Par3 itself also interacts with aPKC and has a demonstrated role in regulating aPKC localization, additional studies are required to establish whether AMPK regulates Par3 and aPKC independently or whether the three proteins participate in a single pathway (46). It has been reported that Par3 phosphorylation by upstream kinases such as Rassf5 and Ndr regulates its localization; consequently, it is reasonable to hypothesize that AMPK may serve a similar function (47,48).

Several separate studies have shown that AMPK regulates the activities of members of the GTP-binding Rho family proteins. AMPK may interact directly with both RhoA and Rac1 or indirectly regulate Rac1 through its guanine nucleotide exchange factor Tiam1 (49,50). Our results indicate that AMPK may play a similar role for Cdc42, through which it regulates the formation of Cdc42 GTP and thus modulates Cdc42 activity. Additional investigations are required to determine whether AMPK is a direct or indirect regulator of Cdc42. Perhaps not surprisingly, we found that AMPK α1 KD leads to only a 50% reduction in the fraction of Cdc42 that is in the GTP bound state in response to stimuli that initiate junction formation. Consequently, it appears that AMPK may be only one of many regulators of the GTP-bound status of Cdc42 during the process of junction assembly.

The adherens junction protein afadin interacts sequentially during junction assembly with many different junction proteins (5,51,52). It seems logical to suggest that afadin's capacity to participate in these interactions must be dynamically regulated in order to define both spatially and temporally the complements of proteins with which it interacts with during distinct phases of junction assembly. A common mechanism for regulating protein activity or assembly is through phosphorylation. We found by mass spectrometric analysis that afadin is phosphorylated at several different sites. Although there have been a number of studies investigating the phosphorylation status of afadin by upstream kinases, little is understood concerning how afadin phosphorylation specifically affects junction assembly and the ZO-1/afadin interaction (53,54). In concert with previous studies, our data indicate that both AMPK and aPKC may regulate the phosphorylation status of afadin at S1102 and S228 respectively (8). S228 is located in the first Ras-associating domain and S1102 is located in the PDZ domain, and both of these domains are important for protein-protein interactions and regulation. We demonstrated that the absence of phosphorylation at these positions not only perturbs AMPK-mediated junction assembly by decreasing the ability for ZO-1 to localize to the plasma membrane, but that these phosphorylation sites also specifically coordinate the level of ZO-1/afadin interaction. Phosphorylation at S228 and S1102 appear to decrease and increase the extent or stability of ZO-1/afadin interaction, respectively. These results are consistent with the idea that through sequential phosphorylation and dephosphorylation, afadin is able to play a role that may evolve during the course of junction assembly. It will be interesting in future studies to assess whether regulation of afadin's phosphorylation at other sites may similarly help to define afadin's participation in the initiation of junction assembly and in the maturation of the resultant junctional complexes.

The data presented here are consistent with a model in which activation of AMPK promotes Par3 localization to the plasma membrane, which has been shown in the literature to in turn recruit aPKC. AMPK's activation of Cdc42 further leads to aPKC activation. AMPK activity would also result in phosphorylation of afadin at S1102, which would promote its interaction with ZO-1 and thus drive the recruitment of ZO-1 to forming adherens junctions. Activation of aPKC would in turn phosphorylate afadin at S228 (which resides within a predicted aPKC phosphorylation site) to promote ZO-1's dissociation from afadin, thus freeing ZO-1 to interact with transmembrane components of the tight junction and to participate in the maturation of assembling junctions (Fig. 8). It is interesting to note that a conceptually similar mechanism, in which phosphorylation regulates the interaction

between the tight junction protein ZO-2 and 14-3-3 proteins, has recently been shown to regulate the deposition of ZO-2 during junction formation (55). While the scheme presented in Figure 8 encompasses the results of the present studies, additional work will be required to determine whether all of its predictions are observed and whether it is sufficient to account fully for the role of AMPK in junction assembly. Most importantly, future studies will be required to determine whether afadin is subject to sequential phosphorylation by AMPK at S1102 and by aPKC at S228 that cause afadin to interact with ZO-1 and then to dissociate from this interaction, respectively.

Additional investigations are also needed to evaluate more fully whether additional components are required downstream of AMPK to promote AMPK-mediated junction assembly. Since we found that the knockdown of AMPK α1 subunit prevents the redistribution of aPKC and Par3 to the plasma membrane during the Ca^{2+} switch, these findings suggest that AMPK plays an important role in regulating aPKC and Par3 localization in a way that cannot be compensated through other mechanisms activated by the Ca^{2+} switch. In light of the numerous reported regulators of Par3 and aPKC localization, including phosphoinositide-3-kinase, small GTPase Rap1, afadin, Willin, Morg1, and Crumbs3, it seems surprising that AMPK alone would have such a significant role controlling the distribution of Par3 and aPKC under these circumstances (46,56-59). This suggests the interesting possibility that other regulators of aPKC or Par3 localization may depend upon or act downstream of AMPK.

While AMPK is widely understood to serve as an energy sensor and regulator of metabolism, its role as a promoter of adherens and tight junction assembly has been largely considered separately from its energy sensing functions (8-10,60). AMPK activation during the Ca^{2+} switch occurs without any significant changes to cellular energetics, consistent with the paradigm that AMPK's role as an energy sensor is distinct from its role as a regulator of junction assembly (9). The activation of AMPK decreases the activities of several energy consuming cellular processes, such as cell growth and protein/fatty acid synthesis (61). Since junction formation and the maintenance of junction integrity requires dynamic and rapid molecular turnover, which very likely are energy-consuming processes, it thus seems somewhat counter-intuitive that AMPK activation promotes junction assembly (62-64). It is important to note however, that AMPK does not inhibit all energy consuming processes. For example, it plays a significant role in activating glycolysis to increase cellular ATP levels and promote cell survival (60). Perhaps more importantly, although maintaining junction integrity maintenance may be energy consuming at a cellular level and thus unfavorable in the context of an individual cell's energy stress, loss of junction integrity can lead to catastrophic effects at the levels of tissues, organs and organisms. In the kidney, for example, disturbed junctional integrity induced by ischemic injury can lead to severe perturbations in renal tubular fluid and solute absorption, which has the potential to threaten an organism's continued viability. Similarly, loss of junctional integrity as a consequence of intestinal hypoperfusion can lead to severe bacterial infections (43,65). Faced with potentially life-threatening consequences for the organism, it may be advantageous for epithelial cells to expend some energy even in the face of their own energy deprivation so as to preserve junction integrity in order to preserve organ function and survival of the organism. Thus, AMPK's role as an energy sensor may permit it to ensure that energy-requiring processes like junction maintenance continue even in the face of energy deficits.

There appears to be a growing and fascinating convergence between components of cellular machineries that participate in metabolic regulation and in orchestrating junction assembly, further supporting the idea that the two processes are inter-linked. For example, studies examining AMPK's role in regulating metabolic processes demonstrate that aPKC acts downstream of AMPK to promote insulin-induced GLUT4 translocation (66). Our results indicate that aPKC also plays a role in AMPK-mediated junction assembly. It thus appears that AMPK may be able to concurrently increase both cellular glucose levels and to ensure the maintenance of junction integrity to promote cell and tissue survival by signaling through aPKC. It will be interesting to continue to explore both of

these processes in order to elucidate further the extent of the overlap in the pathways that connect AMPK regulation of aPKC activity to metabolism and to junction assembly.

Experimental procedures

Plasmids and cell lines

Par3 KD cells

Gene transfer lentiviral plasmids were purchased from VectorBuilder (pLV U6 shRNA-hPGK puro, VB170922-1159qea). These plasmids allow expression of shRNA directed against PAR3 together with a puromycin resistance marker. Positive control (pLKO.1-puro-CMV-TagRFP, SHC012) and non-target control shRNA (anti-luciferase, VB170922-1161yfy) were purchased from Sigma-Aldrich and VectorBuilder respectively.

Lentiviral vectors were generated with the GIGA Viral Vectors platform. Briefly Lenti-X 293T cells (Clontech®, 632180) were co-transfected with gene transfer lentiviral plasmid, pSPAX2 (Addgene®, Cambridge, MA, USA) plasmid and a VSV-G encoding plasmid (67). Viral supernatants were collected 48h, 72h and 96h post transfection, filtered (0.2µM) and concentrated 100 x by ultracentrifugation. The lentiviral vectors were then titrated with qPCR Lentivirus Titration (Titer) Kit (ABM®, LV900, Richmond, BC, Canada). MDCK cells were transduced with lentiviral vectors (50 TU/cell) allowing the dual expression of shRNA and puromycin resistance protein. Transduced cells were selected with 3µg/mL puromycin (Invivogen, ant-pr-1). The absence of RCL and mycoplasma in cell supernatant was confirmed with qPCR Lentivirus Titration kit and MycoAlert™ PLUS Mycoplasma Detection Kit (Lonza, LT07-710) respectively.

Afadin S216A and S1083A cell lines

The constructs encoding the wild-type *mus musculari*s afadin protein or its S1083A mutant cloned into the pcDNA3.1.neo vector were kindly provided by Dr. Yoshimi Takai. Sequence encoding an HA epitope tag was added to the N-terminus of the encoded protein. A site directed mutation at S216 was introduced by Quikchange Pfu turbo enzyme (Agilent Technologies, Santa Clara, CA). The PCR reaction mixture contained 45ng template DNA, 10x Pfu turbo reaction buffer, 0.26mM of each dNTP, 0.26µM of each primer and 2.5 units of Pfu turbo enzyme in 50µl. The mixture was heated at 95°C for 2 min and then subjected to thermal cycling (18 cycles of 95°C for 30 sec, 55°C for 1 min and 68°C for 11 min). Following subcloning, the gene was fully sequenced to ensure that the mutation was present and that no additional mutations were introduced by PCR. Stable cell lines were generated by transfection of MDCK cells using Lipofectamine 2000 (Invitrogen, Carlsbad, CA) and selection was achieved by culturing cells in medium supplemented with 400mg/ml G418 (Invitrogen).

Antibodies

Rabbit anti-AMPK α1 and anti-pAMPK (T172) were purchased from Cell Signaling (Danvers, MA). Both mouse and rabbit anti-aPKCζ were purchased from Santa Cruz Biotechnology (Dallas, TX). Rabbit anti-Par3 was purchased from Millipore (Billerica, MA). Both mouse and rabbit anti-ZO-1 were purchased from Invitrogen. Rabbit-anti-human-l-afadin was purchased from Sigma-Aldrich (St. Louis, MO). Mouse anti-αHA was purchased from Roche (Indianapolis, IN). Alexa Fluor 488-conjugated goat anti-mouse IgG and Alexa Fluor 594-conjugated goat anti-rabbit IgG were purchased from Molecular Probes (Carlsbad, CA). HRP-conjugated goat anti-mouse IgG and HRP-conjugated goat anti-rabbit IgG were purchased from Jackson ImmunoResearch (Westgrove, PA). Goat anti-mouse IRDye® 800CW and anti-rabbit IRDye® 680CW were purchased from Li-Cor BioSciences (Lincoln, NE).

Cell culture

MDCK cells were maintained in α-MEM (Invitrogen) supplemented with 10% fetal bovine serum (GIBCO-BRL, Grand Island, NY), 2mM L-glutamine (GIBCO-BRL), 50 U/ml penicillin (GIBCO-BRL), and 50mg/ml streptomycin (GIBCO-BRL). All cells were grown in a humidified incubator at 37°C and 5% CO_2 atmosphere and were recently authenticated and tested for contamination.

Ca^{2+} switch and drug exposure experiments

MDCK cells were seeded on tissue culture plastic (for immunoblotting experiments) or on

glass coverslips (for immunofluorescence experiments) in α-MEM containing 1.8 mM Ca^{2+} (normal Ca^{2+} medium) until they formed a confluent monolayer. Cells were then washed four times with PBS before being incubated in Ca^{2+}-free S-MEM (GIBCO-BRL) supplemented with 5% dialyzed fetal bovine serum, 2 mM L-glutamine, 50U/ml penicillin and 50 mg/ml streptomycin for 16 hours. Cells were then returned to normal Ca^{2+}-containing α-MEM medium or exposed to drugs for various time intervals as indicated. AICAR was purchased from Calbiochem (San Diego, CA) and aPKCζ pseudosubstrate (myristoylated) was purchased from Enzo Life Sciences (Farmingdale, NY). Another aPKCζ inhibitor, SC-3098, was purchased from Santa Cruz (Santa Cruz, CA).

Immunofluorescence and quantification of aPKC, Par3, and ZO-1 staining

Cells grown on coverslips were washed twice with PBS and fixed in 100% methanol at room temperature for 7 min. Cells were then washed three times with PBS before being permeabilized in 0.3% Triton X-100/0.15% BSA (permeabilization buffer) in PBS for 15 min at room temperature. These cells were then blocked in GSDB (16% goat serum (Invitrogen), 20 mM sodium phosphate (pH 7.4), 450 mM NaCl, 0.3% Triton X-100) for 30 min at room temperature. Cells were incubated in primary antibody diluted 1:100 in GSDB for 1 h at room temperature and then washed 3 times in permeabilization buffer. The corresponding secondary antibody and Hoechst reagent (Molecular Probes) were diluted 1:200 and 1:10000 in GSDB, respectively. This mixture was added to the cells for a one-hour incubation. Cells were then washed 3 times in PBS before being mounted using Vectashield (Vector Laboratories, Burlingame, CA). The cells were visualized on a Zeiss LSM 780 confocal laser-scanning microscope. Brightness and contrast settings were chosen such that all pixels were in the linear range.

To quantify the average length of aPKC, Par3, or ZO-1 per cell, four fields were randomly selected from each coverslip and the total length of aPKC, Par3, or ZO-1 localized at junction sites in each field was outlined manually and measured using Image J software. An investigator blinded to the conditions of each image performed a confirmatory experiment measuring ZO-1 lengths to ensure that there was no investigator bias. The total number of cell nuclei per field was counted and the average aPKC, Par3, or ZO-1 length per cell was thus calculated. Statistical analysis was performed using the two-tailed Student's t-test.

Immunoblotting

Cells were lysed on ice in 20 mM Tris 7.4, 250 mM sucrose, 50 mM NaCl, 50 mM NaF, 5 mM sodium pyrophosphate, 1 mM sodium orthovanadate, 2 mM fresh dithiothreitol (DTT), 1% Triton, and protease inhibitors (Roche) and sonicated for 30 seconds. Cell lysate was centrifuged at 14,000 rpm at 4°C for 30 min and the supernatant was collected. The proteins were separated by SDS-PAGE using standard protocols and electrophoretically transferred to 0.2-µm or 0.45-µm nitrocellulose membranes (Bio-Rad, Hercules, CA). Proteins separated by Phos-tag SDS-PAGE (Wako, Richmond, VA) according to manufacturer's protocols were transferred to PVDF membranes (Millipore). The membranes were blocked with milk solution (150mM NaCl, 20 mM Tris, 5% milk (w/v), 1% bovine serum albumin (BSA), 0.1& Tween (v/v), pH 7.5) and probed with primary antibody (diluted 1:1000 in 5% BSA solution) and the corresponding IRDye®- or HRP-conjugated secondary (diluted 1:10000) antibodies. The immunoreactive bands were visualized with Odyssey Infrared Scanner (Li-Cor Biosciences) or an enhanced chemiluminescence detection kit (ECL, Amersham Biosciences, Pittsburg, PA). For Par3 WT and KD cells, total protein quantification was obtained using a ChemiDoc MP gel imager (BioRad). No membrane stripping for re-blotting was required as proteins that were of similar molecular weights were be probed with primary antibodies of different species and thus could be visualized with secondary antibodies conjugated to different IRDye®s simultaneously.

Immunoprecipitation

Cells were lysed on ice in 20mM Tris pH 7.4, 150 mM NaCl, 1mM EDTA, 1% Triton and protease inhibitors and sonicated for 15 seconds. Cell lysate was centrifuged at 14,000 rpm at 4°C for 30 min after which the supernatant was collected. Lysates prepared for afadin

immunoprecipitation were incubated with rabbit anti-I-afadin antibody and Protein G agarose beads (Thermo Scientific, Waltham, MA) at 4°C overnight. Beads were collected by centrifugation at 2,000 rpm and the pellets were washed 3 times with lysis buffer and 2 times with PBS for 5 min with rotation at 4°C. Lysates prepared for HA immunoprecipitation were incubated with anti-HA magnetic beads (Pierce, Waltham, MA) for 30 min at room temperature and washed according to manufacturer's protocol. Immunprecipitates and total cell lysates were resolved with 8% SDS-PAGE using standard protocols and analyzed by immunoblotting using the antibodies specified.

Cdc42 Activity Assay

Cdc42 Pak1-binding domain-GST tagged construct (kindly provided by Dr. Martin Schwartz, Yale University) was expressed and collected using glutathione-sepharose 4B beads (Amersham) as previously described (68). Cells were lysed on ice in GST-Fish buffer (10% glycerol, 50mM Tris pH 7.4, 100mM NaCl, 1% NP-40, 2mM $MgCl_2$, 1mM sodium orthovanadate, and protease inhibitors) and sonicated for 5 seconds. Cell lysates were centrifuged at 14,000 rpm at 4°C for 5 min and extracts containing 500µg of total proteins were incubated with 20µg glutathione-bound Pak1 beads (GST-PBD) on a rotator for 15 minutes at 4°C. Beads were collected by centrifugation at 2,000 rpm and washed twice with GST-Fish buffer. Cdc42 bound to GST-PBD and total cell extracts were resolved by 15% SDS-PAGE using standard protocols and analyzed by immunoblotting using the antibodies specified.

Mass Spectrometry Sample Preparation

Immunoprecipitated afadin protein resolved by SDS-PAGE was visualized with Coomassie Blue staining, excised from the gel, and gel fragments were cut into $1mm^3$ pieces. Gel pieces were sequentially washed with fresh solutions containing 50% (v/v) acetonitrile (ACN), 25 mM NH_4HCO_3 and 50% (v/v) ACN, 5mM NH_4HCO_3. Proteins were digested overnight at 37°C in a solution containing 45mM NH_4HCO_3, 5% ACN, and 13.33 ng/ul trypsin (Promega, Madison, WI). Peptides were extracted from gel pieces with 1.67% formic acid (FA) in 66.6% ACN. Samples were loaded onto stage tips assembled in house (2X1.06mm punches of Empore C18 extraction disks (3M, Maplewood, Minnesota) in a 200ul pipette tip), washed twice with 0.5% acetic acid, and eluted with 80% acetonitrile, 0.5% acetic acid. In-solution peptide labeling was performed using 100 mM TEAB, 4% formaldehyde (CH_2O or CD_2O), 0.6M cyanoborohydride, 1% (v/v) ammonia and 5% (v/v) formic acid in water. Peptides from cells subjected to CS conditions were labeled using CD_2O and those from cells under LCM conditions were labeled using CH_2O. Samples were then combined in a 1:1 ratio. 1ul was taken from each sample and mixed with 19% formic acid, 27 mM sodium phosphate, pH 8.2 and 0.02% TFA for relative quantification of total afadin peptides (non-enriched sample). The remaining phosphopeptides were enriched by reconstitution in 20ul of binding buffer (50% ACN, 0.5% TFA) and loaded onto stage tips assembled in-house (1x0.6mm punch of Empore C18 extraction disks in a 200ul pipette tip, loaded with 400ug of Titanshere TiO2 microspheres (GL Sciences, Tokyo, Japan)). Tips were washed twice with binding buffer and once with 80% ACN, 0.1% FA. Peptides were eluted with 1% NH_4OH followed by 80% ACN, 0.1% FA. Peptides were dried and reconstituted in a solution of 19% formic acid, 27 mM sodium phosphate, pH 8.2, and 0.02% TFA for LC/MS/MS analysis.

Chromatographic separation was performed on an a Waters nanoAcquity system with a vented split configuration on a 32 mm 150 µm ID trap column packed in-house with 3 µm ReproSil-Pur C18-AQ 120A resin (Dr. Maisch) and a 200 mm 75 µm ID PicoFrit analytical column (New Objective, Altamonte Springs, FL) packed in-house with 1.9 µm ReproSil-Pur C18-AQ 120A resin (Dr. Maisch) using a nonlinear, 90-minute gradient from 5% to 95% ACN (with 0.1% FA) and analyzed on a LTQ Orbitrap Velos (Thermo Fisher Scientific). Peptides were detected in data dependent mode using a Top 10 data dependent acquisition method and HCD dissociation. Data were searched using Maxquant v1.5.1.0. The ratios of TiO_2 enriched phosphopeptides were normalized according to the averages of all afadin non-phosphopeptide ratios from the corresponding non-enriched samples. Putative

kinases were determined by motif scan according to MIT Scansite 4.0 (41).

Acknowledgements

We are grateful to Dr. Yoshimi Takai (Kobe University Graduate School of Medicine) for providing the afadin construct. We thank all of the members of the Caplan laboratory for insightful advice and discussions. This work was supported by NIH grants DK17433 and DK072612[#]. JW was supported in part by the American Association for University Women American Fellowship. BMG was supported by DGE1122492.

Competing interests

The authors declare that they have no conflicts of interest with the contents of this article.

[#]The content is solely the responsibility of the authors and does not necessarily represent the official views of the National Institutes of Health.

References

1. Matter, K., and Balda, M. S. (2003) Signalling to and from tight junctions. *Nat Rev Mol Cell Biol* **4**, 225-236
2. Cereijido, M., Valdes, J., Shoshani, L., and Contreras, R. G. (1998) Role of tight junctions in establishing and maintaining cell polarity. *Annu Rev Physiol* **60**, 161-177
3. Farkas, A. E., Capaldo, C. T., and Nusrat, A. (2012) Regulation of epithelial proliferation by tight junction proteins. *Ann N Y Acad Sci* **1258**, 115-124
4. Van Itallie, C. M., Aponte, A., Tietgens, A. J., Gucek, M., Fredriksson, K., and Anderson, J. M. (2013) The N and C termini of ZO-1 are surrounded by distinct proteins and functional protein networks. *J Biol Chem* **288**, 13775-13788
5. Ooshio, T., Kobayashi, R., Ikeda, W., Miyata, M., Fukumoto, Y., Matsuzawa, N., Ogita, H., and Takai, Y. (2010) Involvement of the interaction of afadin with ZO-1 in the formation of tight junctions in Madin-Darby canine kidney cells. *J Biol Chem* **285**, 5003-5012
6. Fanning, A. S., and Anderson, J. M. (2009) Zonula occludens-1 and -2 are cytosolic scaffolds that regulate the assembly of cellular junctions. *Ann N Y Acad Sci* **1165**, 113-120
7. Miranda, L., Carpentier, S., Platek, A., Hussain, N., Gueuning, M. A., Vertommen, D., Ozkan, Y., Sid, B., Hue, L., Courtoy, P. J., Rider, M. H., and Horman, S. (2010) AMP-activated protein kinase induces actin cytoskeleton reorganization in epithelial cells. *Biochem Biophys Res Commun* **396**, 656-661
8. Zhang, L., Jouret, F., Rinehart, J., Sfakianos, J., Mellman, I., Lifton, R. P., Young, L. H., and Caplan, M. J. (2011) AMP-activated protein kinase (AMPK) activation and glycogen synthase kinase-3beta (GSK-3beta) inhibition induce Ca2+-independent deposition of tight junction components at the plasma membrane. *J Biol Chem* **286**, 16879-16890
9. Zhang, L., Li, J., Young, L. H., and Caplan, M. J. (2006) AMP-activated protein kinase regulates the assembly of epithelial tight junctions. *Proc Natl Acad Sci U S A* **103**, 17272-17277
10. Zheng, B., and Cantley, L. C. (2007) Regulation of epithelial tight junction assembly and disassembly by AMP-activated protein kinase. *Proc Natl Acad Sci U S A* **104**, 819-822
11. Caplan, M. J., Seo-Mayer, P., and Zhang, L. (2008) Epithelial junctions and polarity: complexes and kinases. *Curr Opin Nephrol Hypertens* **17**, 506-512
12. Iden, S., Misselwitz, S., Peddibhotla, S. S., Tuncay, H., Rehder, D., Gerke, V., Robenek, H., Suzuki, A., and Ebnet, K. (2012) aPKC phosphorylates JAM-A at Ser285 to promote cell contact maturation and tight junction formation. *J Cell Biol* **196**, 623-639
13. Jain, S., Suzuki, T., Seth, A., Samak, G., and Rao, R. (2011) Protein kinase Czeta phosphorylates occludin and promotes assembly of epithelial tight junctions. *Biochem J* **437**, 289-299
14. Smith, C. A., Lau, K. M., Rahmani, Z., Dho, S. E., Brothers, G., She, Y. M., Berry, D. M., Bonneil, E., Thibault, P., Schweisguth, F., Le Borgne, R., and McGlade, C. J. (2007) aPKC-mediated phosphorylation regulates asymmetric membrane localization of the cell fate determinant Numb. *EMBO J* **26**, 468-480
15. Hutterer, A., Betschinger, J., Petronczki, M., and Knoblich, J. A. (2004) Sequential roles of Cdc42, Par-6, aPKC, and Lgl in the

establishment of epithelial polarity during Drosophila embryogenesis. *Dev Cell* **6**, 845-854
16. Yamanaka, T., Horikoshi, Y., Suzuki, A., Sugiyama, Y., Kitamura, K., Maniwa, R., Nagai, Y., Yamashita, A., Hirose, T., Ishikawa, H., and Ohno, S. (2001) PAR-6 regulates aPKC activity in a novel way and mediates cell-cell contact-induced formation of the epithelial junctional complex. *Genes to cells : devoted to molecular & cellular mechanisms* **6**, 721-731
17. Hirai, T., and Chida, K. (2003) Protein kinase Czeta (PKCzeta): activation mechanisms and cellular functions. *J Biochem* **133**, 1-7
18. Assemat, E., Bazellieres, E., Pallesi-Pocachard, E., Le Bivic, A., and Massey-Harroche, D. (2008) Polarity complex proteins. *Biochim Biophys Acta* **1778**, 614-630
19. Citi, S., Guerrera, D., Spadaro, D., and Shah, J. (2014) Epithelial junctions and Rho family GTPases: the zonular signalosome. *Small GTPases* **5**, 1-15
20. Ooshio, T., Fujita, N., Yamada, A., Sato, T., Kitagawa, Y., Okamoto, R., Nakata, S., Miki, A., Irie, K., and Takai, Y. (2007) Cooperative roles of Par-3 and afadin in the formation of adherens and tight junctions. *J Cell Sci* **120**, 2352-2365
21. Martinez-Estrada, O. M., Villa, A., Breviario, F., Orsenigo, F., Dejana, E., and Bazzoni, G. (2001) Association of junctional adhesion molecule with calcium/calmodulin-dependent serine protein kinase (CASK/LIN-2) in human epithelial caco-2 cells. *J Biol Chem* **276**, 9291-9296
22. Seo-Mayer, P. W., Thulin, G., Zhang, L., Alves, D. S., Ardito, T., Kashgarian, M., and Caplan, M. J. (2011) Preactivation of AMPK by metformin may ameliorate the epithelial cell damage caused by renal ischemia. *Am J Physiol Renal Physiol* **301**, F1346-1357
23. Takiar, V., Nishio, S., Seo-Mayer, P., King, J. D., Jr., Li, H., Zhang, L., Karihaloo, A., Hallows, K. R., Somlo, S., and Caplan, M. J. (2011) Activating AMP-activated protein kinase (AMPK) slows renal cystogenesis. *Proc Natl Acad Sci U S A* **108**, 2462-2467
24. Stuart, R. O., and Nigam, S. K. (1995) Regulated assembly of tight junctions by protein kinase C. *Proc Natl Acad Sci U S A* **92**, 6072-6076
25. Fukuhara, T., Shimizu, K., Kawakatsu, T., Fukuyama, T., Minami, Y., Honda, T., Hoshino, T., Yamada, T., Ogita, H., Okada, M., and Takai, Y. (2004) Activation of Cdc42 by trans interactions of the cell adhesion molecules nectins through c-Src and Cdc42-GEF FRG. *J Cell Biol* **166**, 393-405
26. Honda, T., Shimizu, K., Kawakatsu, T., Fukuhara, A., Irie, K., Nakamura, T., Matsuda, M., and Takai, Y. (2003) Cdc42 and Rac small G proteins activated by trans-interactions of nectins are involved in activation of c-Jun N-terminal kinase, but not in association of nectins and cadherin to form adherens junctions, in fibroblasts. *Genes to cells : devoted to molecular & cellular mechanisms* **8**, 481-491
27. Etienne-Manneville, S., and Hall, A. (2001) Integrin-mediated activation of Cdc42 controls cell polarity in migrating astrocytes through PKCzeta. *Cell* **106**, 489-498
28. Shin, Y. J., Kim, E. H., Roy, A., and Kim, J. H. (2013) Evidence for a novel mechanism of the PAK1 interaction with the Rho-GTPases Cdc42 and Rac. *PLoS One* **8**, e71495
29. Parsons, M., Monypenny, J., Ameer-Beg, S. M., Millard, T. H., Machesky, L. M., Peter, M., Keppler, M. D., Schiavo, G., Watson, R., Chernoff, J., Zicha, D., Vojnovic, B., and Ng, T. (2005) Spatially distinct binding of Cdc42 to PAK1 and N-WASP in breast carcinoma cells. *Mol Cell Biol* **25**, 1680-1695
30. Shin, K., Fogg, V. C., and Margolis, B. (2006) Tight junctions and cell polarity. *Annual review of cell and developmental biology* **22**, 207-235
31. Mack, N. A., Porter, A. P., Whalley, H. J., Schwarz, J. P., Jones, R. C., Khaja, A. S., Bjartell, A., Anderson, K. I., and Malliri, A. (2012) beta2-syntrophin and Par-3 promote an apicobasal Rac activity gradient at cell-cell junctions by differentially regulating Tiam1 activity. *Nat Cell Biol* **14**, 1169-1180
32. Horikoshi, Y., Suzuki, A., Yamanaka, T., Sasaki, K., Mizuno, K., Sawada, H., Yonemura, S., and Ohno, S. (2009) Interaction between PAR-3 and the aPKC-PAR-6 complex is indispensable for apical domain development of epithelial cells. *J Cell Sci* **122**, 1595-1606
33. Theodore, L., Derossi, D., Chassaing, G., Llirbat, B., Kubes, M., Jordan, P., Chneiweiss, H., Godement, P., and Prochiantz, A. (1995)

Intraneuronal delivery of protein kinase C pseudosubstrate leads to growth cone collapse. *J Neurosci* **15**, 7158-7167
34. Laudanna, C., Mochly-Rosen, D., Liron, T., Constantin, G., and Butcher, E. C. (1998) Evidence of zeta protein kinase C involvement in polymorphonuclear neutrophil integrin-dependent adhesion and chemotaxis. *J Biol Chem* **273**, 30306-30315
35. Lim, S., Choi, J. W., Kim, H. S., Kim, Y. H., Yea, K., Heo, K., Kim, J. H., Kim, S. H., Song, M., Kim, J. I., Ryu, S. H., and Suh, P. G. (2008) A myristoylated pseudosubstrate peptide of PKC-zeta induces degranulation in HMC-1 cells independently of PKC-zeta activity. *Life Sci* **82**, 733-740
36. Andreeva, A. Y., Krause, E., Muller, E. C., Blasig, I. E., and Utepbergenov, D. I. (2001) Protein kinase C regulates the phosphorylation and cellular localization of occludin. *J Biol Chem* **276**, 38480-38486
37. Kinoshita, E., Kinoshita-Kikuta, E., and Koike, T. (2009) Separation and detection of large phosphoproteins using Phos-tag SDS-PAGE. *Nat Protoc* **4**, 1513-1521
38. Ong, S. E., and Mann, M. (2006) A practical recipe for stable isotope labeling by amino acids in cell culture (SILAC). *Nat Protoc* **1**, 2650-2660
39. Boersema, P. J., Raijmakers, R., Lemeer, S., Mohammed, S., and Heck, A. J. (2009) Multiplex peptide stable isotope dimethyl labeling for quantitative proteomics. *Nat Protoc* **4**, 484-494
40. Mazanek, M., Mituloviae, G., Herzog, F., Stingl, C., Hutchins, J. R., Peters, J. M., and Mechtler, K. (2007) Titanium dioxide as a chemo-affinity solid phase in offline phosphopeptide chromatography prior to HPLC-MS/MS analysis. *Nat Protoc* **2**, 1059-1069
41. Obenauer, J. C., Cantley, L. C., and Yaffe, M. B. (2003) Scansite 2.0: Proteome-wide prediction of cell signaling interactions using short sequence motifs. *Nucleic Acids Res* **31**, 3635-3641
42. Edelblum, K. L., and Turner, J. R. (2009) The tight junction in inflammatory disease: communication breakdown. *Curr Opin Pharmacol* **9**, 715-720
43. Devarajan, P. (2006) Update on mechanisms of ischemic acute kidney injury. *J Am Soc Nephrol* **17**, 1503-1520
44. Martin, T. A., and Jiang, W. G. (2009) Loss of tight junction barrier function and its role in cancer metastasis. *Biochim Biophys Acta* **1788**, 872-891
45. Chen, J., and Zhang, M. (2013) The Par3/Par6/aPKC complex and epithelial cell polarity. *Experimental cell research* **319**, 1357-1364
46. Ishiuchi, T., and Takeichi, M. (2011) Willin and Par3 cooperatively regulate epithelial apical constriction through aPKC-mediated ROCK phosphorylation. *Nat Cell Biol* **13**, 860-866
47. Yang, R., Kong, E., Jin, J., Hergovich, A., and Puschel, A. W. (2014) Rassf5 and Ndr kinases regulate neuronal polarity through Par3 phosphorylation in a novel pathway. *J Cell Sci* **127**, 3463-3476
48. Khazaei, M. R., and Puschel, A. W. (2009) Phosphorylation of the par polarity complex protein Par3 at serine 962 is mediated by aurora a and regulates its function in neuronal polarity. *J Biol Chem* **284**, 33571-33579
49. Moon, S., Han, D., Kim, Y., Jin, J., Ho, W. K., and Kim, Y. (2014) Interactome analysis of AMP-activated protein kinase (AMPK)-alpha1 and -beta1 in INS-1 pancreatic beta-cells by affinity purification-mass spectrometry. *Sci Rep* **4**, 4376
50. You, G. Y., Lee, J. O., Kim, J. H., Kim, N., Lee, S. K., Moon, J. W., Jie, S., Lee, H. J., Kim, S. J., Park, S. H., and Kim, H. S. (2013) Tiam-1, a GEF for Rac1, plays a critical role in metformin-mediated glucose uptake in C2C12 cells. *Cell Signal* **25**, 2558-2565
51. Monteiro, A. C., Sumagin, R., Rankin, C. R., Leoni, G., Mina, M. J., Reiter, D. M., Stehle, T., Dermody, T. S., Schaefer, S. A., Hall, R. A., Nusrat, A., and Parkos, C. A. (2013) JAM-A associates with ZO-2, afadin, and PDZ-GEF1 to activate Rap2c and regulate epithelial barrier function. *Mol Biol Cell* **24**, 2849-2860
52. Ikeda, W., Nakanishi, H., Miyoshi, J., Mandai, K., Ishizaki, H., Tanaka, M., Togawa, A., Takahashi, K., Nishioka, H., Yoshida, H., Mizoguchi, A., Nishikawa, S., and Takai, Y. (1999) Afadin: A key molecule essential for structural organization of cell-cell junctions of

polarized epithelia during embryogenesis. *J Cell Biol* **146**, 1117-1132
53. Elloul, S., Kedrin, D., Knoblauch, N. W., Beck, A. H., and Toker, A. (2014) The adherens junction protein afadin is an AKT substrate that regulates breast cancer cell migration. *Mol Cancer Res* **12**, 464-476
54. Radziwill, G., Erdmann, R. A., Margelisch, U., and Moelling, K. (2003) The Bcr kinase downregulates Ras signaling by phosphorylating AF-6 and binding to its PDZ domain. *Mol Cell Biol* **23**, 4663-4672
55. Amaya, E., Alarcon, L., Martin-Tapia, D., Cuellar-Perez, F., Cano-Cortina, M., Ortega-Olvera, J. M., Cisneros, B., Rodriguez, A. J., Gamba, G., and Gonzalez-Mariscal, L. (2019) Activation of the Ca(2+) sensing receptor and the PKC/WNK4 downstream signaling cascade induces incorporation of ZO-2 to tight junctions and its separation from 14-3-3. *Mol Biol Cell* **30**, 2377-2398
56. Shi, S. H., Jan, L. Y., and Jan, Y. N. (2003) Hippocampal neuronal polarity specified by spatially localized mPar3/mPar6 and PI 3-kinase activity. *Cell* **112**, 63-75
57. Choi, W., Harris, N. J., Sumigray, K. D., and Peifer, M. (2013) Rap1 and Canoe/afadin are essential for establishment of apical-basal polarity in the Drosophila embryo. *Mol Biol Cell* **24**, 945-963
58. Hayase, J., Kamakura, S., Iwakiri, Y., Yamaguchi, Y., Izaki, T., Ito, T., and Sumimoto, H. (2013) The WD40 protein Morg1 facilitates Par6-aPKC binding to Crb3 for apical identity in epithelial cells. *J Cell Biol* **200**, 635-650
59. Schluter, M. A., Pfarr, C. S., Pieczynski, J., Whiteman, E. L., Hurd, T. W., Fan, S., Liu, C. J., and Margolis, B. (2009) Trafficking of Crumbs3 during cytokinesis is crucial for lumen formation. *Mol Biol Cell* **20**, 4652-4663
60. Mihaylova, M. M., and Shaw, R. J. (2011) The AMPK signalling pathway coordinates cell growth, autophagy and metabolism. *Nat Cell Biol* **13**, 1016-1023
61. Shackelford, D. B., and Shaw, R. J. (2009) The LKB1-AMPK pathway: metabolism and growth control in tumour suppression. *Nat Rev Cancer* **9**, 563-575
62. Shen, L., Weber, C. R., and Turner, J. R. (2008) The tight junction protein complex undergoes rapid and continuous molecular remodeling at steady state. *J Cell Biol* **181**, 683-695
63. Fletcher, S. J., Iqbal, M., Jabbari, S., Stekel, D., and Rappoport, J. Z. (2014) Analysis of occludin trafficking, demonstrating continuous endocytosis, degradation, recycling and biosynthetic secretory trafficking. *PLoS One* **9**, e111176
64. Schnittler, H., Taha, M., Schnittler, M. O., Taha, A. A., Lindemann, N., and Seebach, J. (2014) Actin filament dynamics and endothelial cell junctions: the Ying and Yang between stabilization and motion. *Cell Tissue Res* **355**, 529-543
65. Rahman, S. H., Ammori, B. J., Holmfield, J., Larvin, M., and McMahon, M. J. (2003) Intestinal hypoperfusion contributes to gut barrier failure in severe acute pancreatitis. *J Gastrointest Surg* **7**, 26-36
66. Lee, J. O., Lee, S. K., Jung, J. H., Kim, J. H., You, G. Y., Kim, S. J., Park, S. H., Uhm, K. O., and Kim, H. S. (2011) Metformin induces Rab4 through AMPK and modulates GLUT4 translocation in skeletal muscle cells. *J Cell Physiol* **226**, 974-981
67. Emi, N., Friedmann, T., and Yee, J. K. (1991) Pseudotype formation of murine leukemia virus with the G protein of vesicular stomatitis virus. *J Virol* **65**, 1202-1207
68. Meller, N., Irani-Tehrani, M., Kiosses, W. B., Del Pozo, M. A., and Schwartz, M. A. (2002) Zizimin1, a novel Cdc42 activator, reveals a new GEF domain for Rho proteins. *Nat Cell Biol* **4**, 639-647

Figure Legends

Figure 1 AMPK regulates aPKC localization during junction assembly

(A) Confluent MDCK cells were stably transfected with empty pSUPER vector (AMPK WT) or pSUPER containing shRNA directed against AMPK α1 (AMPK α1 KD) and were incubated in media containing 5 μM Ca^{2+} (low calcium media, LCM) for 16h. Fresh LCM or media containing 1.8 mM Ca^{2+} (calcium switch) were introduced for 2h. Cells were fixed and immunostained for aPKC. Scale bar: 30 μm. (B) Quantification of aPKC localization at sites of

junction assembly. Data were analyzed for each experimental condition based on four randomly obtained views from three independent coverslips. Error bars represent the s.e.m. of the length of aPKC per cell within each of the four selected fields of view. The asterisks (*) denote that there is a significant difference due to the calcium switch ($p < 0.05$) compared to LCM conditions based on the Student's *t*-test. (C) Confluent WT MDCK cells were incubated in media containing 5 μM Ca^{2+} (low calcium media, LCM) for 16h. Fresh LCM with or without 2mM AICAR was introduced for 1h. Cells undergoing the calcium switch were introduced to media containing 1.8 mM Ca^{2+} for 1h. Cells were fixed and immunostained for aPKC. Scale bar: 30 μm. Arrowheads indicate sites of junction assembly. (D) Quantification of aPKC localization at sites of junction assembly. Data were analyzed for each experimental condition based on four randomly obtained views from three independent coverslips. Error bars represent the s.e.m. of the length of aPKC per cell within each of the four selected fields of view. The asterisks (**) denote that there is a significant difference due to the presence of AICAR or the calcium switch ($p < 0.01$) compared to LCM conditions based on the Student's *t*-test.

Figure 2. AMPK regulates the level of GTP-bound Cdc42

(A) Confluent MDCK cells were stably transfected with pSUPER containing shRNA against the AMPK α1 isoform (AMPK α1 KD) or the empty vector (AMPK WT) and incubated in media containing 5 μM Ca^{2+} (low calcium media, LCM) for 16h. Fresh LCM with or without 2mM AICAR or media containing 1.8 mM Ca^{2+} (calcium switch) were introduced for 2h. Cell lysates from each condition was obtained and analyzed for GTP-bound Cdc42 via a pulldown assay as described in Materials and Methods. Equal amounts of precipitates were then separated on SDS-PAGE and probed with anti-Cdc42 antibody. Cells lysates were analyzed by Western blot with the Cdc42 antibody. (B) Quantification of the immunoreactive signal for Cdc42 in precipitates normalized to the level of Cdc42. Data were analyzed for each experimental condition based on three independent experiments and represent mean intensity relative to LCM(WT) level ± S.E.M. The asterisks denote that there is a significant difference due to the presence of AICAR ($p < 0.01$) or the calcium switch ($p < 0.0001$) compared to LCM conditions based on the Student's *t*-test. (C) Confluent MDCK cells were incubated in media containing 5 μM Ca^{2+} (low calcium media, LCM) for 16h. Fresh LCM with or without 2mM AICAR or media containing 1.8 mM Ca^{2+} (calcium switch) were introduced for 2h. Cell lysates from each condition was obtained and analyzed for GTP-bound Cdc42 via a pulldown assay as described in Materials and Methods. Equal amounts of precipitates were then separated on SDS-PAGE and probed with anti-Cdc42 antibody. Cells lysates were analyzed by Western blot with the Cdc42 antibody. (D) Quantification of the immunoreactive signal for Cdc42 in precipitates normalized to the level of Cdc42. Data were analyzed for each experimental condition based on three independent experiments and represent mean intensity relative to LCM(WT) level ± S.E.M. The asterisks denote that there is a significant difference due to the presence of AICAR ($p < 0.01$) or the calcium switch ($p < 0.0001$) compared to LCM conditions based on the Student's *t*-test.

Figure 3. Par3 expression is important for both calcium switch and AMPK-mediated ZO-1 localization to the plasma membrane

MDCK cells grown to confluency were incubated in media containing 5 μM Ca^{2+} (low calcium media, LCM) for 16h prior to being introduced to fresh LCM, LCM containing 2mM AICAR or media containing 1.8mM Ca^{2+} (normal calcium media, NCM) for one or two hours as indicated. (A, C) Cells were fixed and immunostained for ZO-1. Scale bar: 30 μm. Arrowheads indicate sites of junction assembly. (B, D) Quantification of ZO-1 localization at sites of junction assembly. Data were analyzed for each experimental condition based on four randomly obtained views from three independent coverslips. Error bars represent the s.e.m. of the length of Par3 per cell within each of the four selected fields of view. The asterisks (***) denote that there is a significant difference due to the presence of AICAR ($p < 0.01$) or the calcium switch ($p < 0.01$) compared to LCM conditions based on the Student's *t*-test.

Figure 4. AICAR promotes the localization of Par3 to the plasma membrane

(A) Confluent MDCK cells were incubated in media containing 5 μM Ca^{2+} (low calcium media, LCM) for 16h. Fresh LCM with or without 2mM AICAR was introduced for 1h. Cells undergoing the calcium switch was introduced to media containing 1.8 mM Ca^{2+} for 1h. Cells were fixed and immunostained for Par3. Scale bar: 30 μm. Arrowheads indicate sites of junction assembly. (B) Quantification of Par3 localization at sites of junction assembly. Data were analyzed for each experimental condition based on four randomly obtained views from three independent coverslips. Error bars represent the s.e.m. of the length of Par3 per cell within each of the four selected fields of view. The asterisks (**) denote that there is a significant difference due to the presence of AICAR ($p < 0.01$) or the calcium switch ($p < 0.0001$) compared to LCM conditions based on the Student's *t*-test.

Figure 5. aPKC inhibition decreases both calcium switch- and AMPK-mediated ZO-1 localization to sites of junction assembly and affects the level of interaction between ZO-1 and afadin during junction assembly

Confluent MDCK cells were incubated in media containing 5 μM Ca^{2+} (low calcium media, LCM) for 16h. Cells without aPKC inhibition (− aPKCi) were introduced to fresh LCM, switched to media containing 1.8mM Ca^{2+} (normal calcium media, NCM), or 1 mM AICAR for the indicated time points (upper panel). Cells subject to aPKC inhibition (+ aPKCi) were pre-treated with the indicated concentration of aPKC psuedosubstrate inhibitor for 2h before being introduced to fresh LCM, NCM, or 1mM AICAR containing aPKC inhibitor for the indicated quantity and time points. (A) Cells were fixed and immunostained for ZO-1. Scale bar: 30 μm. (B, C) Quantification of ZO-1 localization at sites of junction assembly. Data were analyzed for each experimental condition based on four randomly obtained views from three independent coverslips. Error bars represent the s.e.m. of the length of ZO-1 per cell within each of the four selected fields of view. (D) Cells lysates were probed with the indicated antibodies by Western blot analysis. (E, G) Cell lysates from each condition were obtained and immunoprecipitated using antibody directed against afadin and Protein G agarose beads. Equal amounts of immunoprecipitates were then separated on SDS-PAGE and probed with anti-ZO-1 antibody. Total cells lysates were simultaneously subjected to immuobloting using anti-ZO-1 and afadin antibodies. (F, H) Quantification of the immunoreactive signal for ZO-1 in immunoprecipitates normalized to the level of immunoprecipitated afadin. Data were analyzed for each experimental condition based on five independent experiments and represent mean intensity relative to LCM level ± S.E.M. The asterisks denote that there is a significant difference due to the presence of aPKC inhibition ($p < 0.01$) or the calcium switch ($p < 0.001$) compared to LCM conditions based on the Student's *t*-test.

Figure 6. Afadin phosphorylation is an important component of AICAR- and calcium switch-mediated junction assembly

(A) Confluent MDCK cells were incubated in media containing 5 μM Ca^{2+} (low calcium media, LCM) for 16h. Fresh LCM with or without 2mM AICAR or media containing 1.8 mM Ca^{2+} (calcium switch) were introduced for 2h. Alkaline phosphatase treatment was performed at 37°C for 1h. Cell lysates were separated by phos-tag acrylamide gel electrophoresis. Western blot analysis was used to probe for protein expression with the anti-Afadin antibody. (B and E) Confluent MDCK cells stably transfected with HA-tagged afadin corresponding with the wild-type *mus musculus* cDNA sequence (upper panels) or containing the S216A or S1083A mutations (lower panels) were incubated in media containing 5 μM Ca2+ (low calcium media, LCM) for 16h. Fresh LCM with or without 2mM AICAR or media containing 1.8mM Ca^{2+} (calcium switch) were introduced for 2h. Cells were fixed and immunostained for ZO-1. Scale bar: 30 μm. (C, D, F and G) Quantification of ZO-1 localization at sites of junction assembly. Data were analyzed for each experimental condition based on four randomly obtained views from three independent coverslips. Error bars represent the s.e.m. of the length of ZO-1 per cell within each of the four selected fields of view. The asterisks (****) denote that there is a significant difference due to the calcium switch or AICAR

($p < 0.001$) compared to LCM conditions based on the Student's *t*-test.

Figure 7. S216A and S1083A mutations in afadin influence its interaction with ZO-1

(A and C) Confluent MDCK cells stably transfected with HA-tagged afadin corresponding with the wild-type *mus musculus* cDNA sequence, the S216A or the S1083A mutation were incubated in media containing 5 μM Ca2+ (low calcium media, LCM) for 16h. Fresh LCM or media containing 1.8mM Ca^{2+} (calcium switch) for 2h. Cell lysates from each condition were obtained and immunoprecipitated with HA-antibody conjugated beads. Equal amounts of immunoprecipitates were then separated on SDS-PAGE and probed with anti-ZO-1 and anti-HA antibody. Total cells lysates were simultaneously subjected to immuobloting using anti-ZO-1 antibody. (B and D) Quantification of the immunoreactive signal for ZO-1 in immunoprecipitates normalized to the level of immunoprecipitated HA-tagged afadin. Data were analyzed for each experimental condition based on three independent experiments and represent mean intensity relative to LCM (WT) level ± S.E.M. The asterisks (***) denote that there is a significant difference due to the presence of the calcium switch ($p < 0.001$) compared to LCM conditions based on the Student's *t*-test.

Figure 8. Schematic diagram of proposed model for how AMPK regulates Par polarity complex proteins

A) Activation of AMPK leads to 1) Par3 translocation to the plasma membrane, 2) aPKC translocation to the plasma membrane and phosphorylation either directly (2a) or via activation of GTP-bound Cdc42 (2b), and 3) Afadin phosphorylation at S1102. B) Phosphorylated afadin in turn interacts with ZO-1 to promote its localization to the nascent adherens junction, while activated aPKC phosphorylates afadin at S228 to C) promote the dissociation of afadin from ZO-1 such that ZO-1 may then translocate to the nascent tight junction.

Table 1. Selected peptides from native afadin (uniprot: F1PSU6) identified by LC-MS/MS

Confluent WT MDCK cells were incubated in media containing 5 μM Ca^{2+} (low calcium media, LCM) for 16h. Cells undergoing the calcium switch were introduced to media containing 1.8 mM Ca^{2+} for 2h. Phosphopeptides were identified through LC-MS/MS analysis of afadin immunoprecipitated from MDCK cells subjected to LCM or CS conditions. Afadin peptides were subjected to titanium dioxide (TiO_2) enrichment to isolate phosphopeptides. Unambiguous assignment of phosphorylation sites are indicated in underlined S. Normalized ratios were obtained by comparing the phosphopeptide ratios of TiO_2-enriched samples relative to the ratios of their non-phosphorylated counterparts (n = 6). Putative kinases were determined by searching MIT Scansite 4.0.

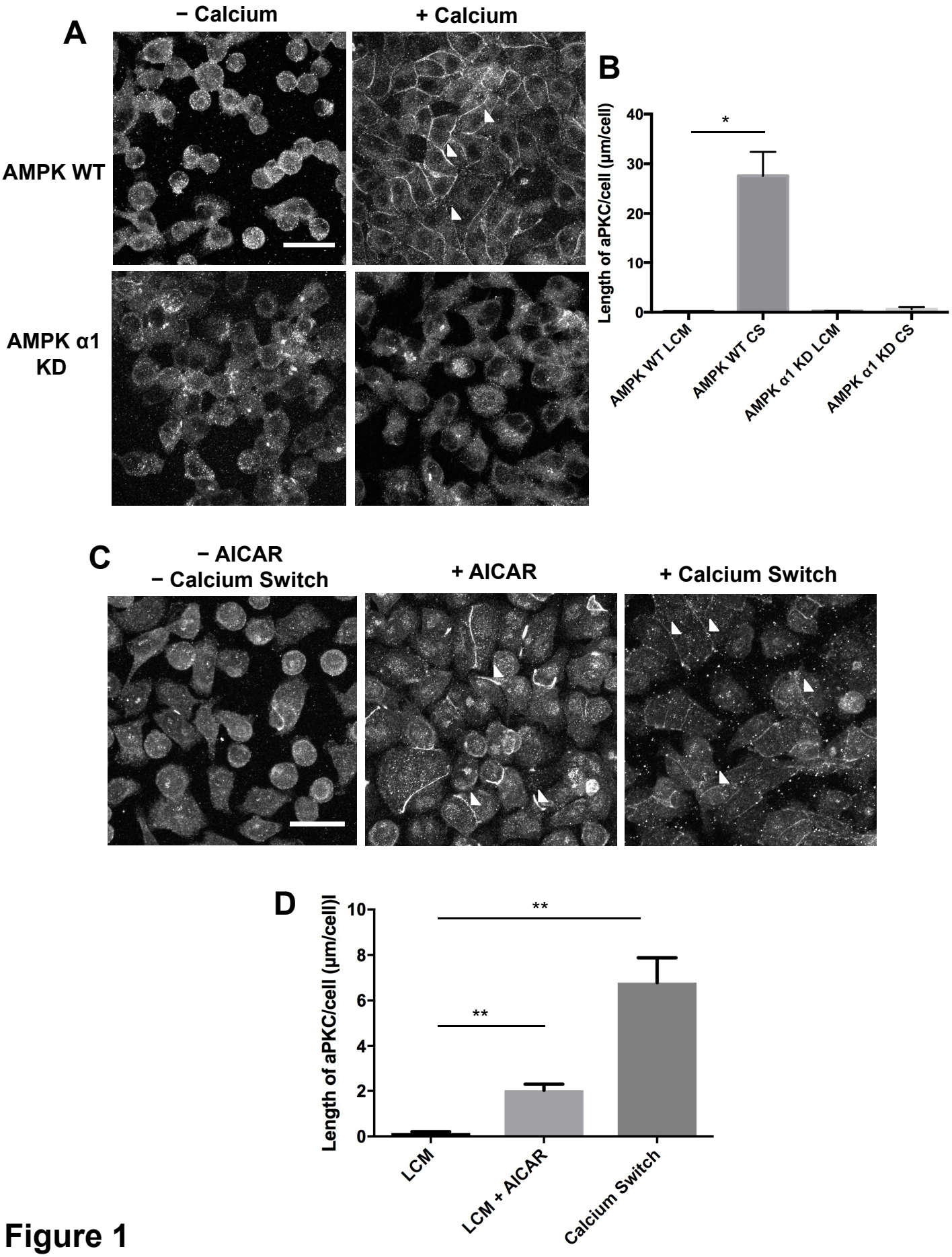
A
− Calcium
+ Calcium
AMPK WT
AMPK α1 KD
B
Length of aPKC/cell (µm/cell)
40
30
20
10
0
*
AMPK WT LCM
AMPK WT CS
AMPK α1 KD LCM
AMPK α1 KD CS
C
− AICAR
− Calcium Switch
+ AICAR
+ Calcium Switch
D
Length of aPKC/cell (µm/cell)
10
8
6
4
2
0
**
**
LCM
LCM + AICAR
Calcium Switch

Figure 1

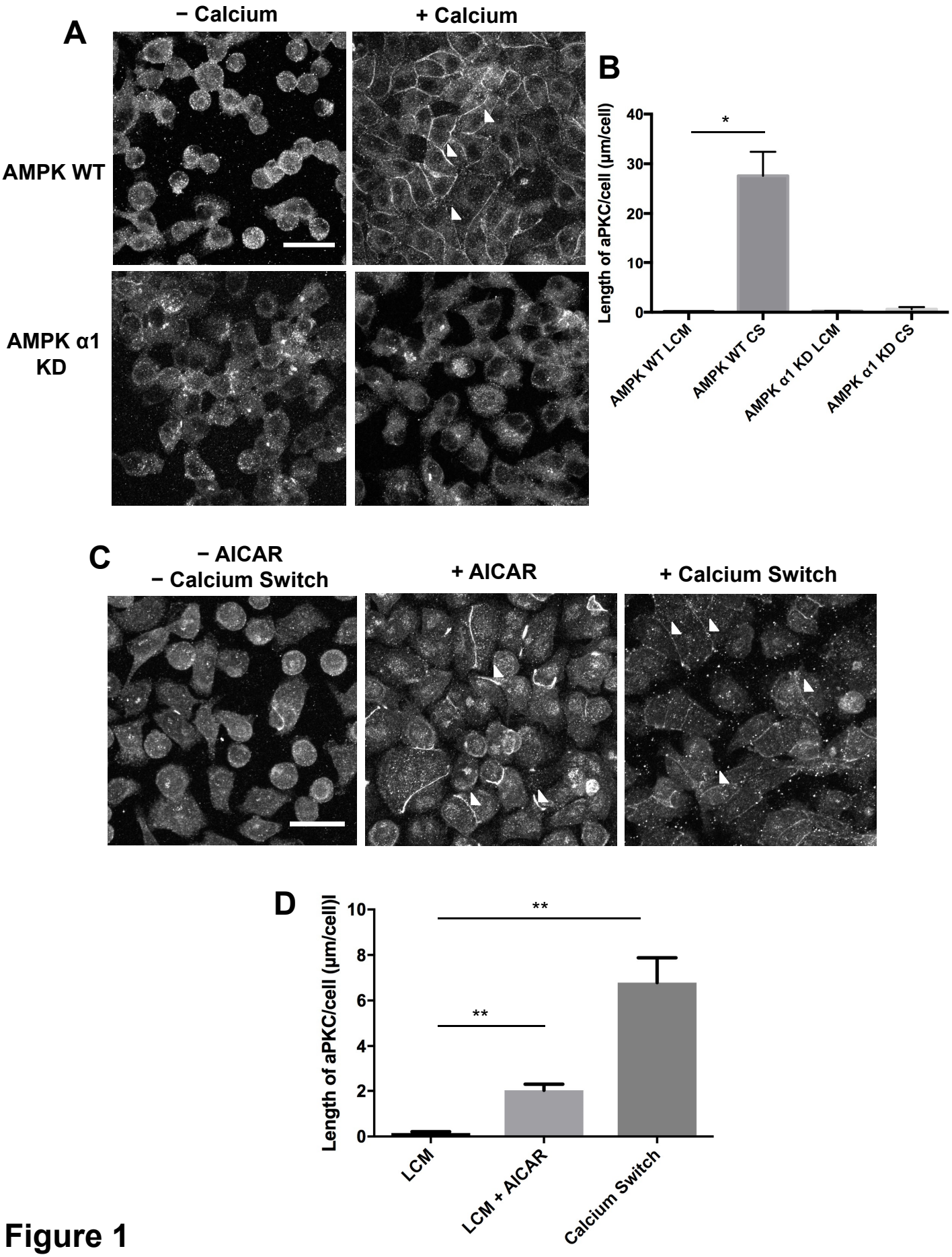
A
− Calcium
+ Calcium
AMPK WT
AMPK α1 KD
B
Length of aPKC/cell (µm/cell)
40
30
20
10
0
*
AMPK WT LCM
AMPK WT CS
AMPK α1 KD LCM
AMPK α1 KD CS
C
− AICAR
− Calcium Switch
+ AICAR
+ Calcium Switch
D
Length of aPKC/cell (µm/cell)
10
8
6
4
2
0
**
**
LCM
LCM + AICAR
Calcium Switch

Figure 1

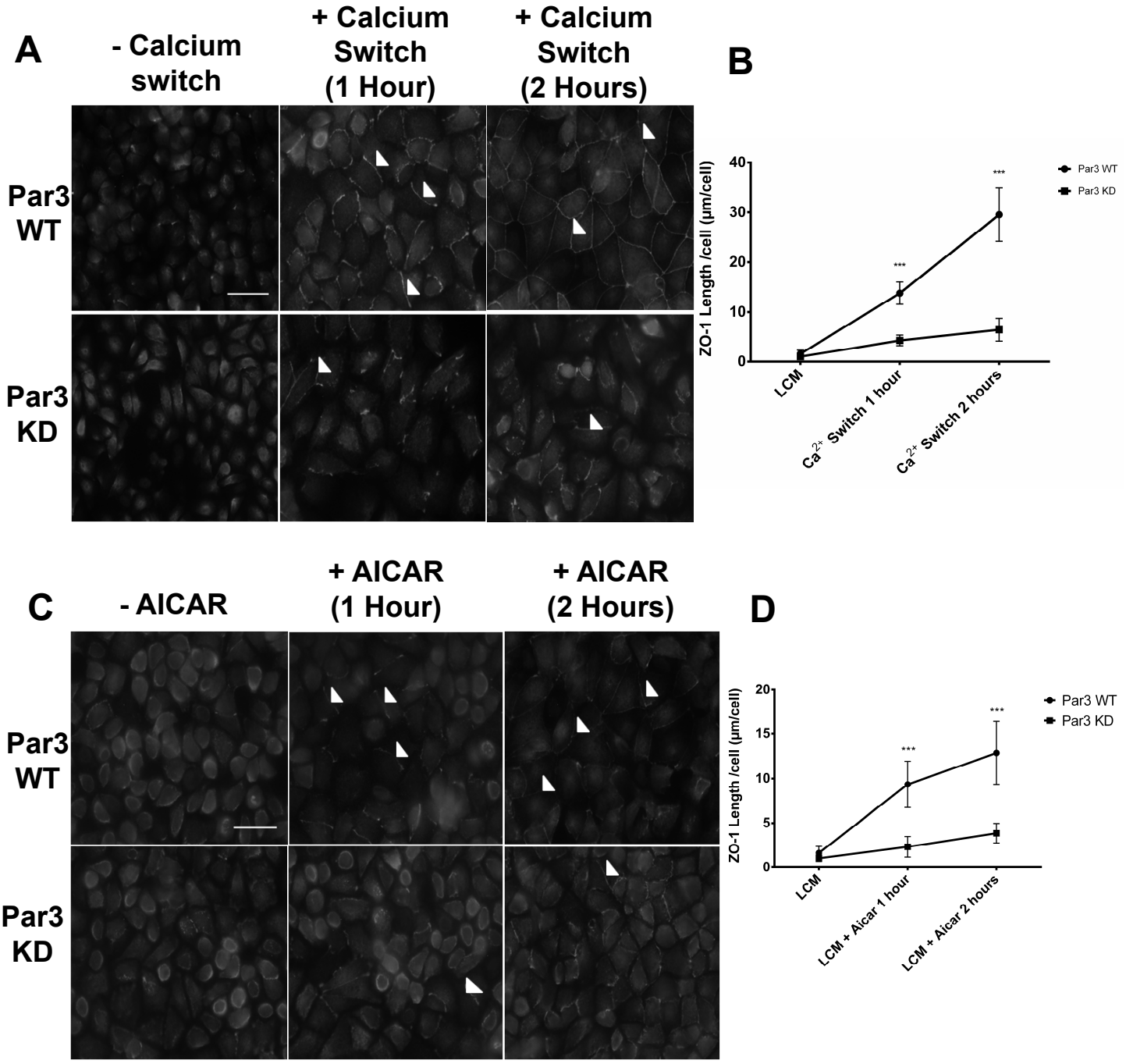
A
- Calcium switch
+ Calcium Switch (1 Hour)
+ Calcium Switch (2 Hours)
Par3 WT
Par3 KD
B
ZO-1 Length /cell (µm/cell)
40
30
20
10
0
***
***
Par3 WT
Par3 KD
LCM
Ca2+ Switch 1 hour
Ca2+ Switch 2 hours
C
- AICAR
+ AICAR (1 Hour)
+ AICAR (2 Hours)
Par3 WT
Par3 KD
D
ZO-1 Length /cell (µm/cell)
20
15
10
5
0
***
***
Par3 WT
Par3 KD
LCM
LCM + Aicar 1 hour
LCM + Aicar 2 hours

Figure 3

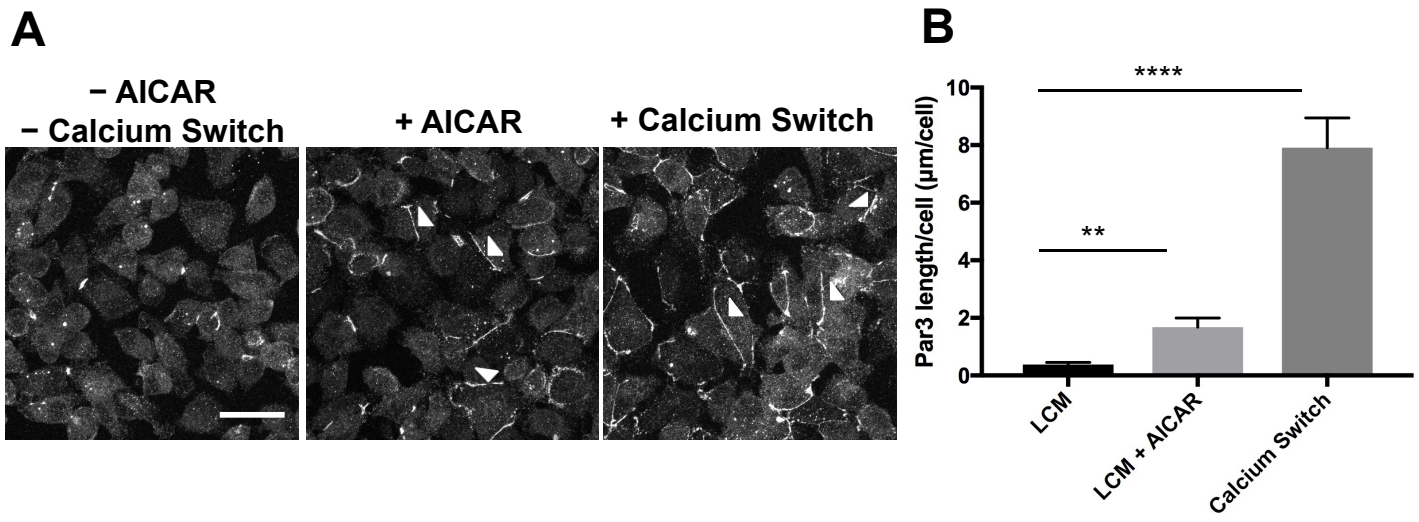
A
− AICAR
− Calcium Switch
+ AICAR
+ Calcium Switch
B
Par3 length/cell (µm/cell)
10
8
6
4
2
0
****
**
LCM
LCM + AICAR
Calcium Switch

Figure 4

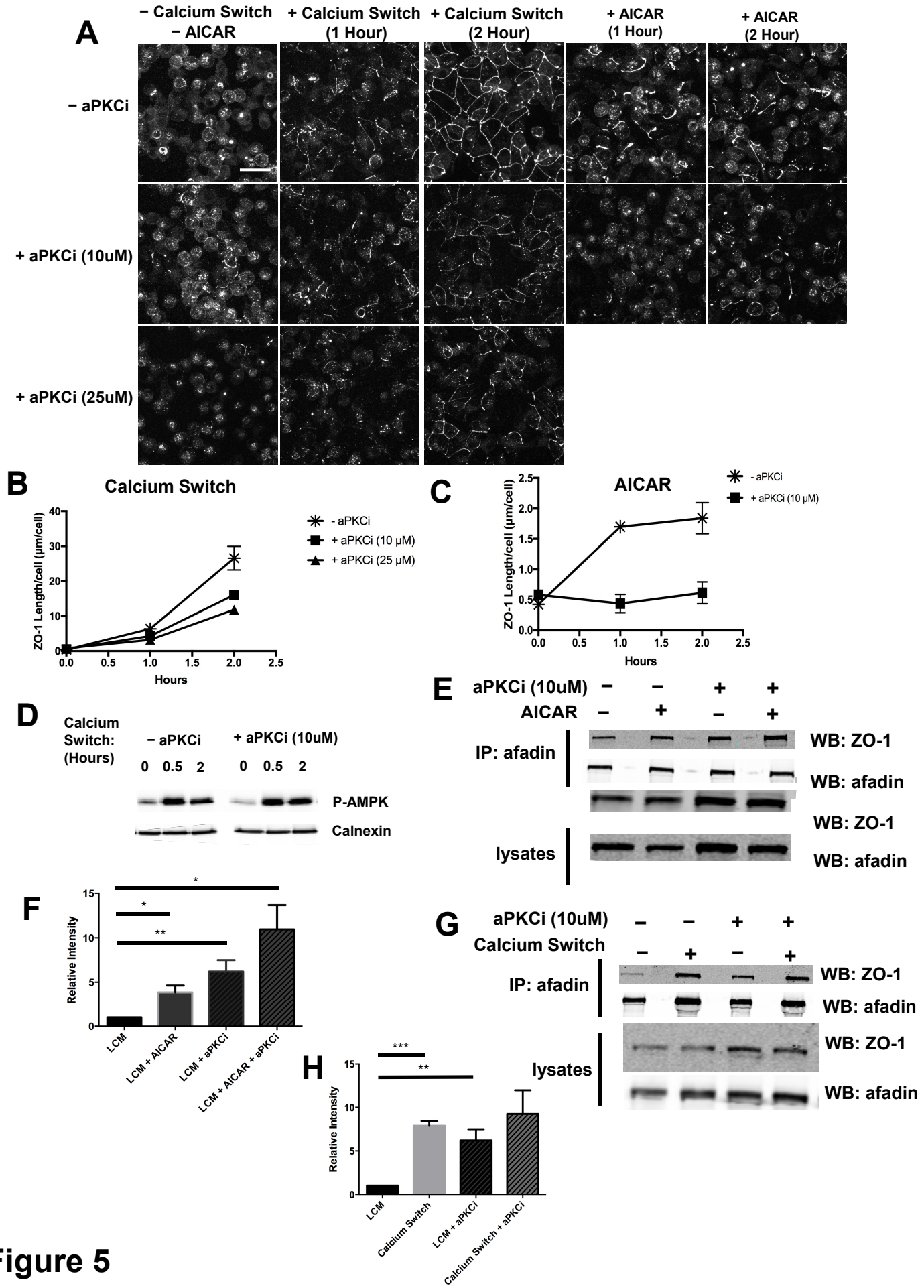
A
− Calcium Switch
− AICAR
+ Calcium Switch
(1 Hour)
+ Calcium Switch
(2 Hour)
+ AICAR
(1 Hour)
+ AICAR
(2 Hour)
− aPKCi
+ aPKCi (10uM)
+ aPKCi (25uM)
B
Calcium Switch
ZO-1 Length/cell (µm/cell)
Hours
- aPKCi
+ aPKCi (10 µM)
+ aPKCi (25 µM)
C
AICAR
ZO-1 Length/cell (µm/cell)
Hours
- aPKCi
+ aPKCi (10 µM)
D
Calcium
Switch:
(Hours)
− aPKCi
+ aPKCi (10uM)
0 0.5 2 0 0.5 2
P-AMPK
Calnexin
E
aPKCi (10uM)
AICAR
IP: afadin
WB: ZO-1
WB: afadin
WB: ZO-1
lysates
WB: afadin
F
Relative Intensity
LCM
LCM + AICAR
LCM + aPKCi
LCM + AICAR + aPKCi
G
aPKCi (10uM)
Calcium Switch
IP: afadin
WB: ZO-1
WB: afadin
lysates
WB: ZO-1
WB: afadin
H
Relative Intensity
LCM
Calcium Switch
LCM + aPKCi
Calcium Switch + aPKCi

Figure 5

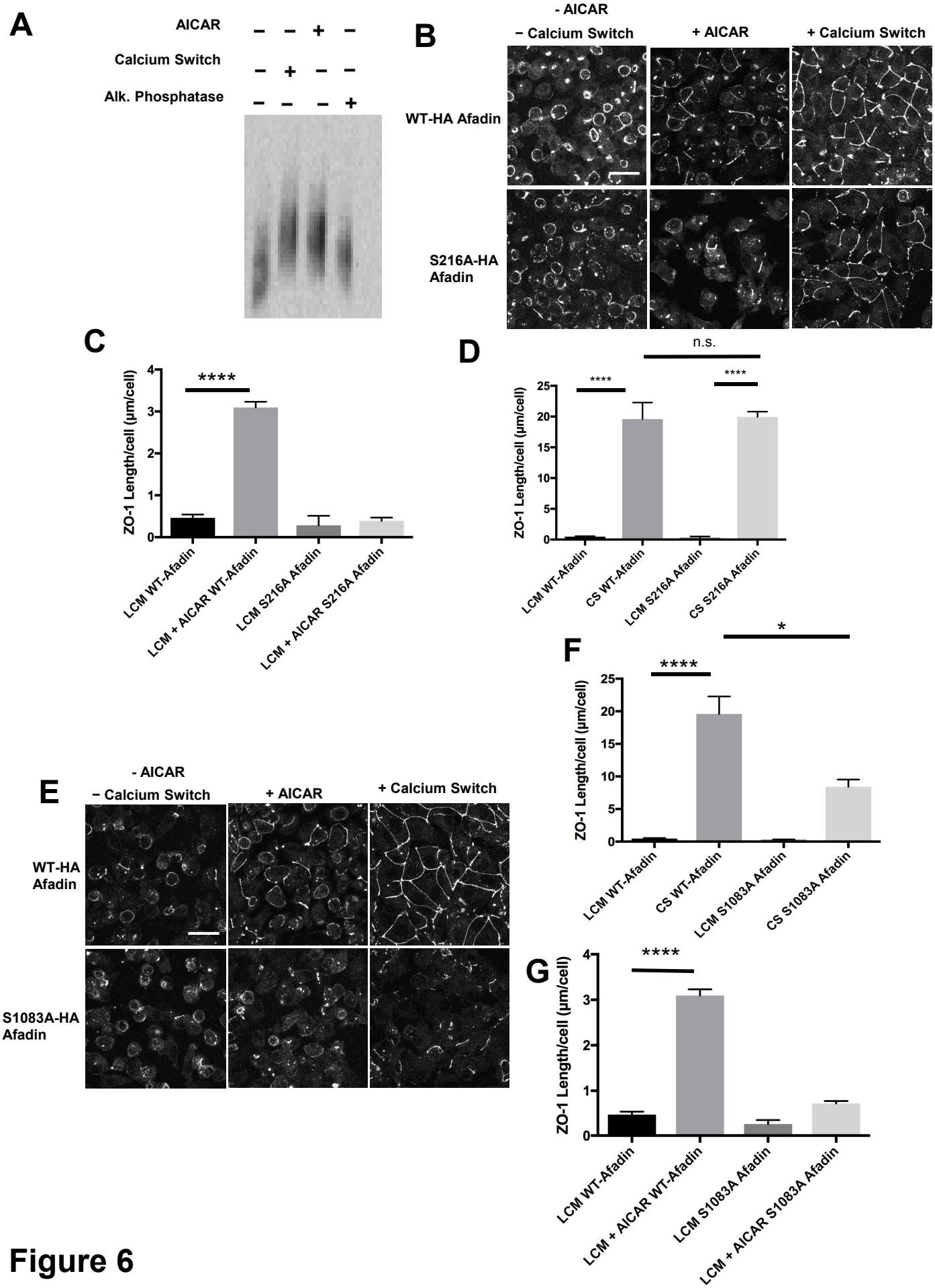
A
AICAR
Calcium Switch
Alk. Phosphatase
B
- AICAR
− Calcium Switch
+ AICAR
+ Calcium Switch
WT-HA Afadin
S216A-HA Afadin
C
ZO-1 Length/cell (µm/cell)
****
LCM WT-Afadin
LCM + AICAR WT-Afadin
LCM S216A Afadin
LCM + AICAR S216A Afadin
D
n.s.
****
****
ZO-1 Length/cell (µm/cell)
LCM WT-Afadin
CS WT-Afadin
LCM S216A Afadin
CS S216A Afadin
E
- AICAR
− Calcium Switch
+ AICAR
+ Calcium Switch
WT-HA Afadin
S1083A-HA Afadin
F
*
****
ZO-1 Length/cell (µm/cell)
LCM WT-Afadin
CS WT-Afadin
LCM S1083A Afadin
CS S1083A Afadin
G
****
ZO-1 Length/cell (µm/cell)
LCM WT-Afadin
LCM + AICAR WT-Afadin
LCM S1083A Afadin
LCM + AICAR S1083A Afadin

Figure 6

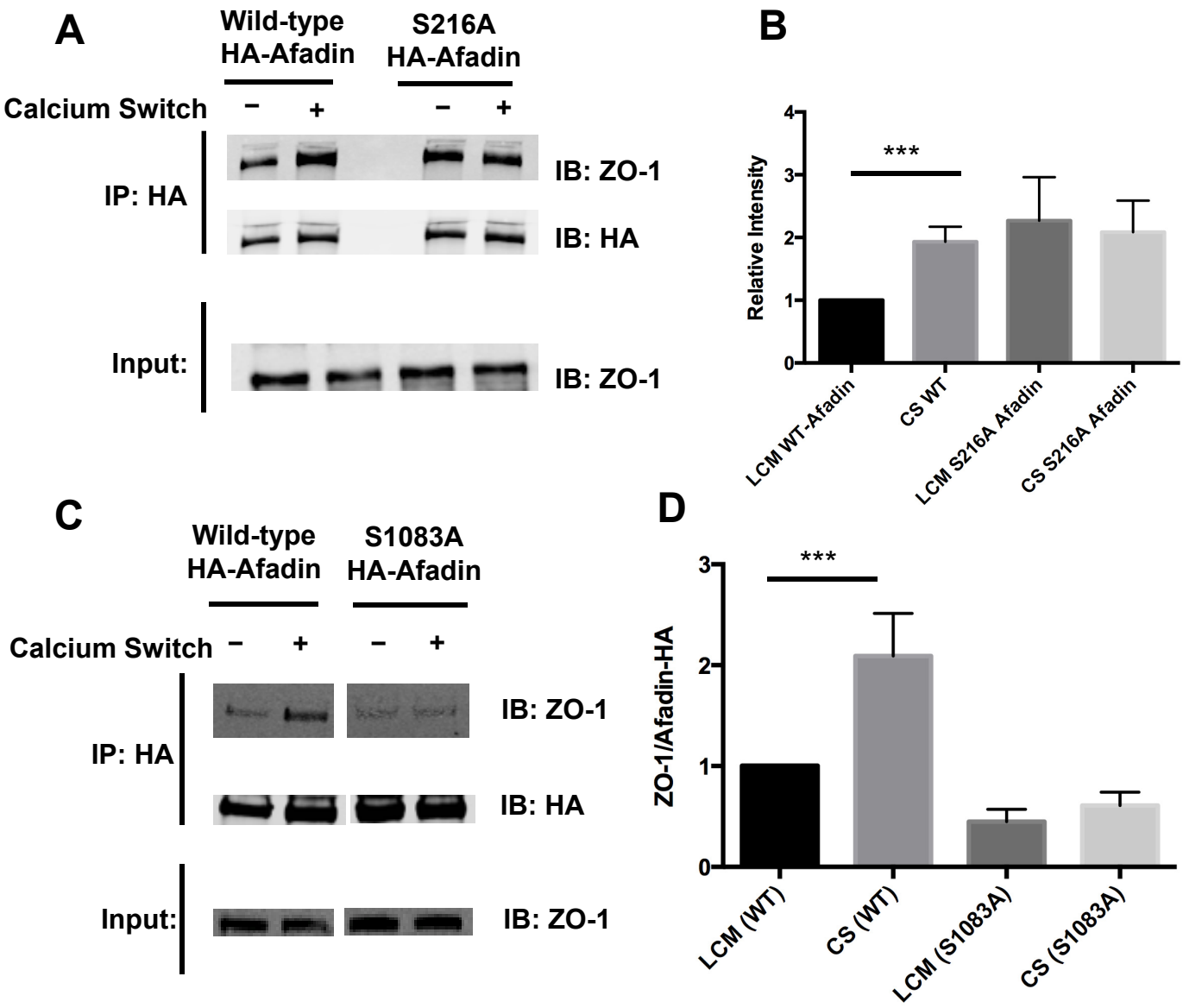
A
Wild-type HA-Afadin
S216A HA-Afadin
Calcium Switch
– + – +
IP: HA
IB: ZO-1
IB: HA
Input:
IB: ZO-1
B
Relative Intensity
***
LCM WT-Afadin
CS WT
LCM S216A Afadin
CS S216A Afadin
C
Wild-type HA-Afadin
S1083A HA-Afadin
Calcium Switch
– + – +
IP: HA
IB: ZO-1
IB: HA
Input:
IB: ZO-1
D
ZO-1/Afadin-HA
***
LCM (WT)
CS (WT)
LCM (S1083A)
CS (S1083A)

Figure 7

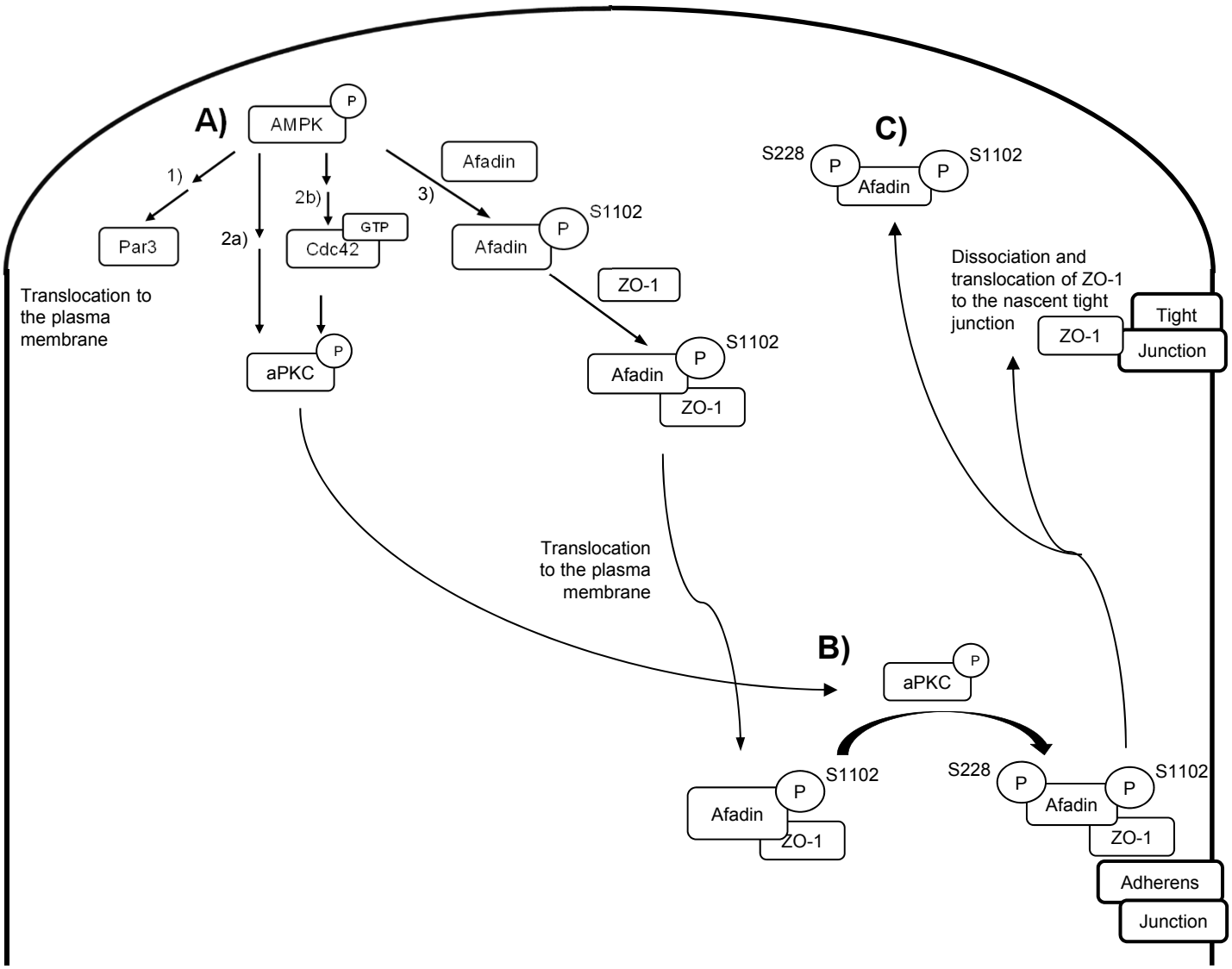
A)
AMPK
P
1)
Par3
2a)
2b)
Cdc42
GTP
3)
Afadin
Afadin
P
S1102
ZO-1
Translocation to the plasma membrane
aPKC
P
Afadin
P
S1102
ZO-1
Translocation to the plasma membrane
B)
aPKC
P
Afadin
P
S1102
ZO-1
S228
P
Afadin
P
S1102
ZO-1
C)
S228
P
Afadin
P
S1102
Dissociation and translocation of ZO-1 to the nascent tight junction
ZO-1
Tight Junction
Adherens Junction

Figure 8

Position	Afadin Peptide (dog)	m/z	CS/LCM Normalized Ratio (n=6)	CS/LCM Ratio 95% CI	Putative Kinase
S216	214-TISNPEVVMK-223	1196.551	1.703	1.399-2.007	aPKC
S1083	1081-TSSVVTLEVAK-1091	1212.6	0.9413	0.8695-1.013	AMPK

Table 1